

Ligand-Dependent Conformations and Dynamics of the Serotonin 5-HT_{2A} Receptor Determine Its Activation and Membrane-Driven Oligomerization Properties

Jufang Shan¹, George Khelashvili¹, Sayan Mondal¹, Ernest L. Mehler¹, Harel Weinstein^{1,2*}

1 Department of Physiology and Biophysics, Weill Medical College of Cornell University, New York, New York, United States of America, **2** The HRH Prince Alwaleed Bin Talal Bin Abdulaziz Alsaud Institute for Computational Biomedicine, Weill Medical College of Cornell University, New York, New York, United States of America

Abstract

From computational simulations of a serotonin 2A receptor (5-HT_{2A}R) model complexed with pharmacologically and structurally diverse ligands we identify different conformational states and dynamics adopted by the receptor bound to the full agonist 5-HT, the partial agonist LSD, and the inverse agonist Ketanserin. The results from the unbiased all-atom molecular dynamics (MD) simulations show that the three ligands affect differently the known GPCR activation elements including the toggle switch at W6.48, the changes in the ionic lock between E6.30 and R3.50 of the DRY motif in TM3, and the dynamics of the NPxxY motif in TM7. The computational results uncover a sequence of steps connecting these experimentally-identified elements of GPCR activation. The differences among the properties of the receptor molecule interacting with the ligands correlate with their distinct pharmacological properties. Combining these results with quantitative analysis of membrane deformation obtained with our new method (Mondal et al, Biophysical Journal 2011), we show that distinct conformational rearrangements produced by the three ligands also elicit different responses in the surrounding membrane. The differential reorganization of the receptor environment is reflected in (i)-the involvement of cholesterol in the activation of the 5-HT_{2A}R, and (ii)-different extents and patterns of membrane deformations. These findings are discussed in the context of their likely functional consequences and a predicted mechanism of ligand-specific GPCR oligomerization.

Citation: Shan J, Khelashvili G, Mondal S, Mehler EL, Weinstein H (2012) Ligand-Dependent Conformations and Dynamics of the Serotonin 5-HT_{2A} Receptor Determine Its Activation and Membrane-Driven Oligomerization Properties. PLoS Comput Biol 8(4): e1002473. doi:10.1371/journal.pcbi.1002473

Editor: Dennis R. Livesay, UNC Charlotte, United States of America

Received November 7, 2011; **Accepted** February 26, 2012; **Published** April 19, 2012

Copyright: © 2012 Shan et al. This is an open-access article distributed under the terms of the Creative Commons Attribution License, which permits unrestricted use, distribution, and reproduction in any medium, provided the original author and source are credited.

Funding: The work was supported by the National Institute on Drug Abuse (Grants P01 DA-012923 and R01 DA015170). Computational support was provided by the National Science Foundation Terascale Computing System at the Texas Advanced Computing Center (TG-MCB090132 and TG-MCB080079N), the computer facilities at the Institute of Computational Biomedicine of Weill Cornell Medical College, and New York BlueGene at Brookhaven National Laboratory. The funders had no role in study design, data collection and analysis, decision to publish, or preparation of the manuscript.

Competing Interests: The authors have declared that no competing interests exist.

* E-mail: haw2002@med.cornell.edu

Introduction

Serotonin 2A receptors (5-HT_{2A}R) are a very well characterized family of G-protein coupled receptors (GPCRs) in the amine subclass of rhodopsin-like class A GPCRs [1,2]. The 5-HT_{2A}Rs are targeted by chemically and pharmacologically distinct classes of ligands which include antidepressants, anxiolytics, antiemetics, antipsychotics and anti-migraine agents. Notably, some agonists exhibit hallucinogenic properties [2,3] that have been attributed to specific manners of activation of these receptors [4,5]. Even when they share key structural features, such as the indole moiety of the non-hallucinogen 5-HT and the hallucinogen LSD, the 5-HT_{2A}R ligands have been shown to be able to bind differently to the receptor molecule, and to exhibit different pharmacological properties [2,6,7,8]. Understanding the relation between the different modes of binding of structurally diverse compounds in the 5-HT_{2A}R binding site, and the pharmacological responses they elicit, has therefore been of great interest in the quest for understanding the function of the 5-HT_{2A}R and especially its role in hallucinogenesis [5]. Important clues came from in vivo studies demonstrating that behavioral responses to different 5-HT_{2A}R ligands correlate with distinct transcriptome fingerprints for the

ligands [4]. However, while it remains unclear how ligand binding induces distinct conformational states of the 5-HT_{2A}R, and how this can result in different pharmacological outcomes [5], the significant variability in receptor conformations that can be induced by different ligands has recently been demonstrated for the cognate β_2 -adrenergic receptor [9].

Structural evidence for differential effects of the GPCR ligands in relation to receptor function should be reflected in the variability of rearrangements in the key structural elements involved in the various activation states of the receptors, e.g., the structural motifs/functional microdomains (SM/FMs) [10] (see Figure 1A) that characterize GPCR activation [5,11,12,13]. Specific SM/FMs have been reported from studies of a large variety of GPCRs [10,14,15,16,17], and their dynamic signatures include (i)-the flipping of the toggle switch W6.48 (Trp336, identified here by the Ballesteros-Weinstein generic numbering [18]) in the cluster of conserved aromatic residues in TM5 and TM6, (ii)-the opening/closing of the ionic lock between the DRY motif (D3.49–R3.50–Y3.51) and E6.30, involved in the movement of the intracellular (IC) end of TM6 away from TM3, and (iii)-the dynamics of the conserved NPxxY motif at the IC end of TM7 that connects as well to H8. These are elements of activation



Author Summary

The 5-HT_{2A} receptor for the neurotransmitter serotonin (5-HT) belongs to family A (rhodopsin-like) G-protein coupled receptors (GPCRs), one of the most important classes of membrane proteins that are targeted by an extensive and diverse collection of external stimuli. Recently we learned that different ligands targeting the same GPCR can elicit different biological responses, but the mechanisms remain unknown. We address this fundamental question for the serotonin 5-HT_{2A} receptor, because it is known to respond to the binding of structurally diverse ligands by producing similar stimuli in the cell, and to the binding of quite similar ligands with dramatically different responses. Molecular dynamics simulations of molecular models of the serotonin 5-HT_{2A} receptor in complex with pharmacologically distinct ligands show the dynamic rearrangements of the receptor molecule to be different for these ligands, and the nature and extents of the rearrangements reflect the known pharmacological properties of the ligands as full, partial or inverse activators of the receptor. The different rearrangements of the receptor molecule are shown to produce different rearrangements of the surrounding membrane, a remodeling of the environment that can have differential ligand-determined effects on receptor function and association in the cell's membrane.

common to many GPCRs (see [5,10,11,13,14,15,16,17,19]), and their status in the X-ray structures of various GPCRs has been evaluated [12,20,21,22,23,24,25]. It is still unclear, however, how the binding of different ligands affects these elements of GPCR activation and how they connect to the mechanisms of the ligand-driven receptor oligomerization that has been shown to be critical for GPCR function [26,27,28,29,30,31].

To shed new light on these central mechanistic questions from the perspective of ligand-dependent conformational states involved in the activation and oligomerization of GPCRs in their membrane environment, we performed large-scale molecular dynamics (MD) simulations of 5-HT_{2A}R in complex with ligands exhibiting different pharmacological properties: the full agonist 5-HT, the

partial agonist LSD, and the inverse agonist Ketanserin (KET) (Figure 2A). The simulation results show that the three ligands affect differently the dynamics of SM/FMs monitored in the simulations (Figure 1B), which achieve distinct conformations that are consistent with the pharmacological classification of these ligands. Moreover, the simulations show that the ligand-bound GPCRs produce differential responses in the lipid membrane surrounding the receptor, as reflected in the spatial pattern of the remodeling of membrane thickness. These trajectories reveal as well the modes and effects of direct receptor-cholesterol interaction. Recently we have described the development and implementation of a new method, CTMD (Combined conTinuum and Molecular Dynamics), for quantitative analysis of the membrane remodeling pattern based on MD trajectories [32]. With this method we account for both the membrane remodeling energy and the energy cost of any partial (incomplete) alleviation of the hydrophobic mismatch by this remodeling of the membrane. From the quantitative analysis with CTMD of the simulation results for the monomeric 5-HT_{2A}R we identified ligand-specific local membrane perturbations that can produce different patterns of 5-HT_{2A}R oligomerization driven by hydrophobic mismatch [32]. Our results lead to the prediction that the dimerization interfaces for 5-HT_{2A}R oligomers will be different when the receptor binds ligands with different pharmacological properties (inverse agonist, partial agonist, or agonist), as suggested earlier [27]. Notably, the extent of membrane-driven oligomerization of a 5-HT_{2A}R in the inverse agonist-bound state is predicted to be larger than in the agonist-bound state. These predictions are consistent with previous experimental findings on cognate GPCRs [27,28,31], supporting the link we identify here between ligand-dependent conformational changes in GPCRs and differences in local membrane perturbations.

Results

Agonist-determined dynamics are expressed as an ordered sequence of changes in the SM/FMs of ligand-bound 5-HT_{2A}R

The main dynamic rearrangements observed in the simulations of the 5-HT_{2A}R when it binds each of the ligands, are described

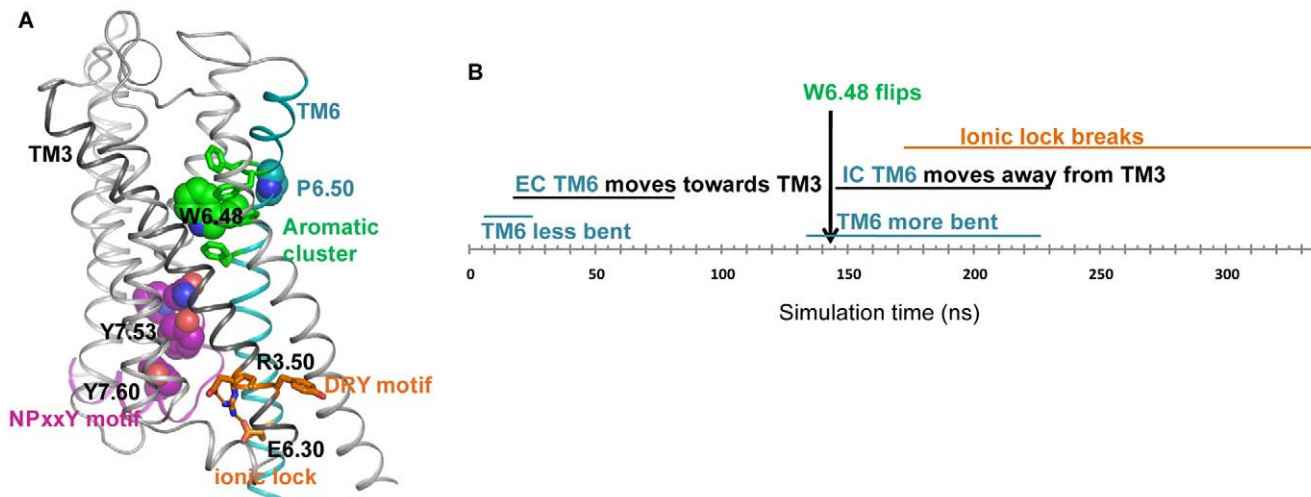


Figure 1. The position and dynamic sequence of structural motifs recognized as functional microdomains (SM/FMs) in the molecular model of the 5-HT_{2A}R. (A) Known structural elements of GPCR activation (SM/FM) in the homology model of the 5-HT_{2A}R. (B) The time-ordered sequence of events identified from the MD simulations of the agonist-bound 5-HT_{2A}R.

doi:10.1371/journal.pcbi.1002473.g001



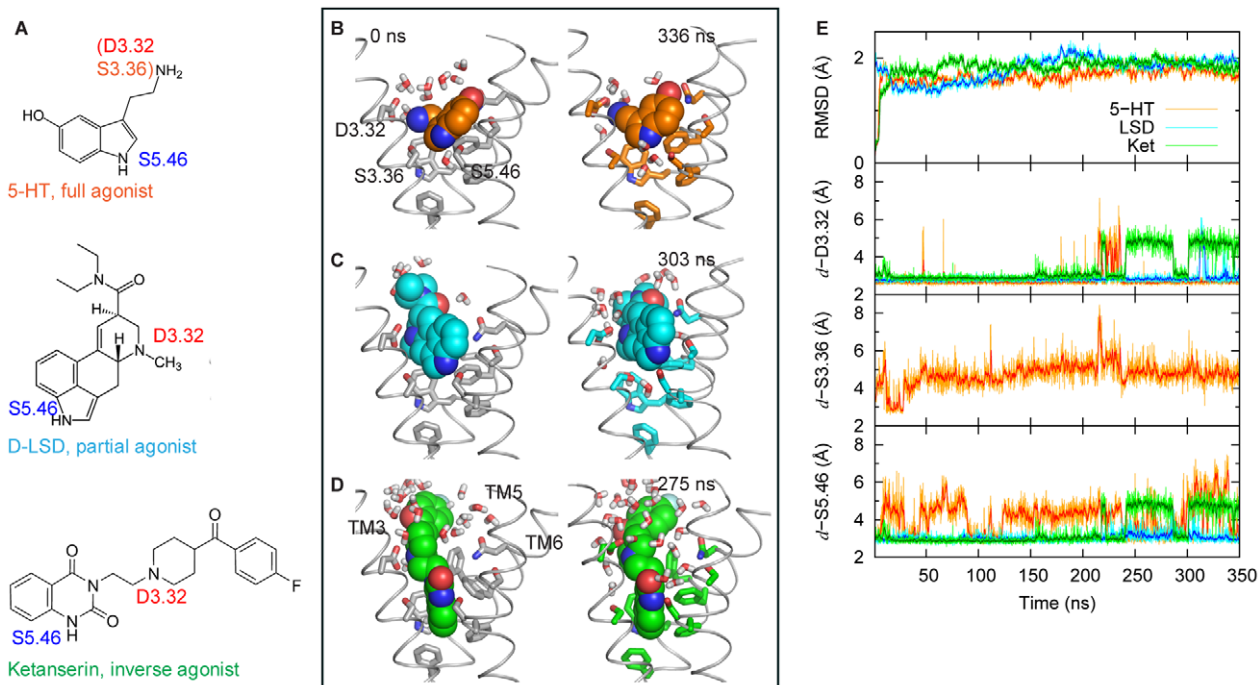


Figure 2. Structures of ligands with different efficacy and their interactions with 5-HT_{2A}R during MD simulations. (A) Chemical structures of 5-HT, LSD and KET. Amines interacting with D3.32, S3.36 or S5.46 [6,7,116,117,118,119] are labeled. (B,C,D) Docking poses in the initial structures (left panels) and during the simulations (right panels) for 5-HT (B), LSD (C) and KET (D), respectively. For clarity, only TM 3, 5 and 6 are shown in grey ribbons. Sidechains of residues D3.32, S3.36, S5.43, S5.46, F5.47, F6.44, W6.48, F6.51, F6.52 and N6.55 are depicted as sticks, and 5-HT (carbons colored in orange), LSD (cyan) and KET (green) are rendered in spheres. Note that, due to its large-size, and because its quinazoline ring penetrates deep into the binding pocket close to W6.48, KET is in direct contact with all the residues in the aromatic cluster, including F5.47. (E) Time-evolution of backbone TM RMSDs of 5-HT_{2A}R (upper panel) and of the distances between the carboxyl/hydroxyl oxygens in D3.32, S3.36 and S5.46 on 5-HT_{2A}R and their interacting amine nitrogens on ligands (see panel A) during the simulations (lower panels). Traces are shown in orange for 5-HT, in cyan for LSD, and in green for KET. Data were collected every 100 ps. Running averages were calculated every 10 data points and are shown in bold shades. N_α atom of 5-HT maintains a salt-bridge with D3.32 and forms an H-bond with S3.36 (Figure S2 in Text S1); N₁ atom of 5-HT forms an H-bond with S5.46 either directly or through a water-bridge.

doi:10.1371/journal.pcbi.1002473.g002

below with reference to the SM/FMs (Figure 1A) identified in this family of GPCRs [5]. The sequential order of the description is determined by the order in which these changes appear in the simulation trajectories of the 5-HT_{2A}R bound to the full agonist 5-HT (Figure 1B).

TM6 and the ionic lock. Figure 1 illustrates the known structural characteristics of GPCR activation and the time-ordered sequence of their occurrence in the simulation of the 5-HT-bound 5-HT_{2A}R. The time-dependent changes in these SM/FMs are detailed in Figure 3. During the initial stages of the simulation, the changes in the orientation of the TM6 segments (before and after the Proline-kink) cause the bend to straighten out (Figure 3A) and the extracellular (EC) end of TM6 to move toward TM3 (Figure 3B and G). This is consistent with a conformational change observed in the crystal structure of β₂AR [25] as well as in experiments [33] associated with β₂AR activation. It is interesting to note that the change in bend angle around P6.50, from 33.2 in the inactive β₂AR (2RH1_chain A) to 25.9 in the active β₂AR (3SN6_chain R), is consistent with the first changes observed in the simulation of 5-HT-bound 5-HT_{2A}R (Figure 3). In addition, the ionic lock (between the DRY motif on the IC end of TM3 and E6.30) changes as shown in Figure 3E: it equilibrates first into a closed form, but in later stages of the trajectory switches back to an open form compatible with the expected agonist-activated conformation; the IC end of TM6 moves away from TM3 (Figure 3D, I). This is remarkable because of the opening of the

ionic lock between the DRY motif and E6.30 is a landmark of GPCR activation [10,34,35,36,37], and the broken ionic lock is evident in an active β₂AR structure stabilized by nanobody [23] as well as an agonist-bound β₂AR in complex with the nucleotide free Gs heterotrimer [25].

The aromatic cluster. From the trajectory, the opening of the ionic lock (Figure 3E) and the movement of the IC end of TM6 (Figure 3D) appear to relate to the rotamer flip of W6.48 from its orientation near-perpendicular to the membrane plane, to a near-parallel one (Figure 3C, J). Such a conformational switch in W6.48 upon GPCR activation has been reported from a variety of experimental studies [36,38], and is observed near the 140 ns time point in the trajectory when the χ₁ angle of W6.48 changes from *g*-to *trans* (Figures 1B, 3C, 3J). When the ring of W6.48 remains parallel to the bilayer for ~1 ns it forms a double pi-pi interaction with both F6.44 and F6.51 (see Figure S1 in Text S1). This may facilitate the change in TM6 kink around P6.50 as suggested earlier [39] which would thus support the opening of the ionic lock by increasing the distance between the IC ends of TM6 and TM3 (Figure 3D).

The NPxxY motif and helix 8. During the first 50 ns of the agonist-bound 5-HT_{2A}R simulation, the conserved NPxxY motif at the IC end of TM7 changes its conformation and spatial relation to H8 (Figure 3F). The dynamics in this SM/FM have been related to GPCR activation [19,22]. In particular, the interdependence of residues at positions 7.53 and 7.60 in the

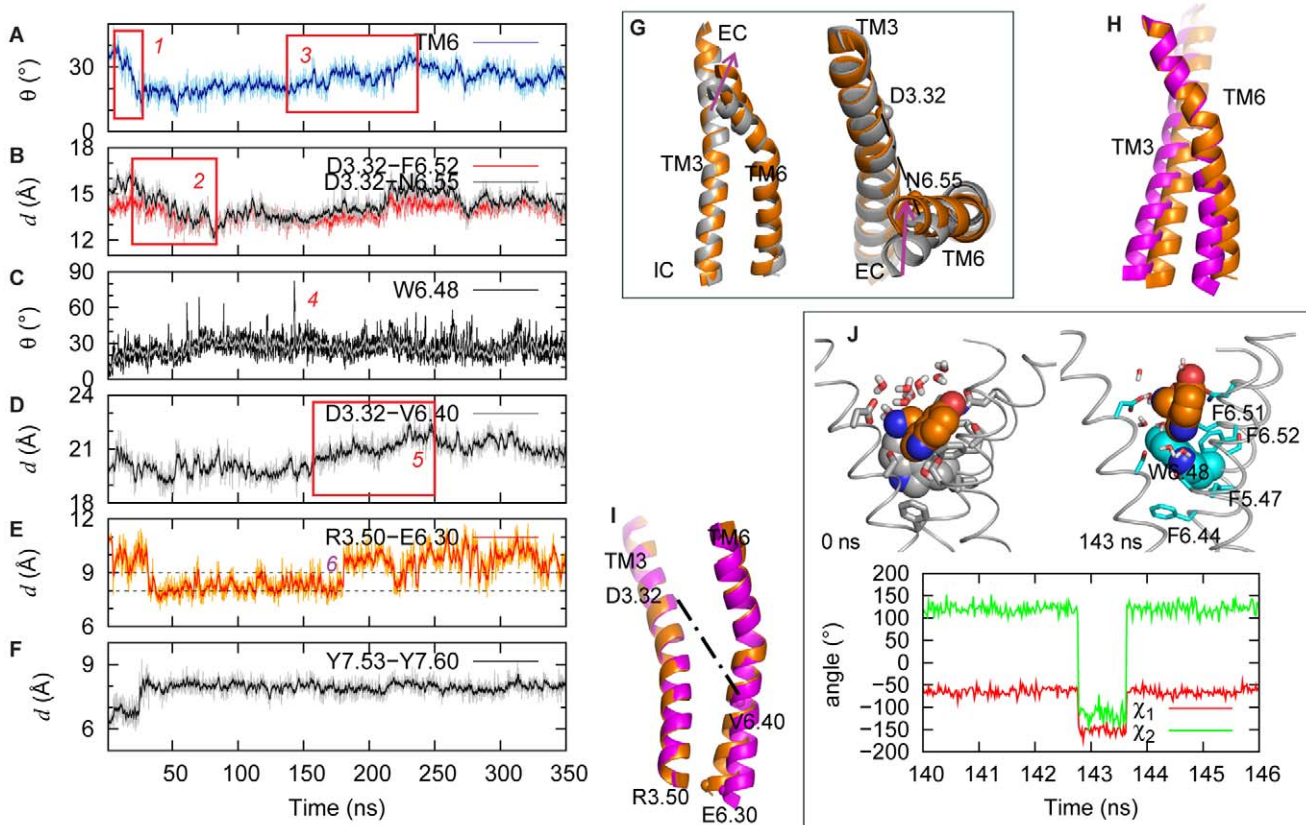


Figure 3. Activation steps of 5-HT_{2A}R bound with 5-HT. (A) Evolution of the bend angle in TM6 around P6.50, highlighting the intervals during which the helix straightens (event 1) and bends (event 3) upon activation. (B) Evolution of the C_α distances between D3.32 and F6.52 (red), and between D3.32 and N6.55 (black), illustrating the interval during which the EC end of TM6 moves towards TM3 (event 2). (C) Evolution of the tilt angle of the toggle switch W6.48 aromatic ring with respect to the membrane normal, showing the time point of W6.48 flipping (event 4). W6.48 becomes parallel to the membrane for ~1 ns at 143 ns (see panel J) with χ_1 angle changing from *g*- to *trans*. (D) Evolution of the C_α distance between D3.32 and V6.40 illustrating the interval when the IC end of TM6 moves away from TM3 (event 5). (E) Dynamics of the ionic lock presented as the evolution of the C_α distance between R3.50 and E6.30. Initially broken ionic lock forms during the first 50 ns, before opening again upon activation at ~170 ns (event 6). (F) Evolution of the C_α distance between Y7.53 and Y7.60. (G) Snapshots from the membrane plane and the EC end, highlighting positions of D3.32 and N6.55 and the distance between them, and showing the initial straightening and motion of TM6 towards TM3 (event 1). Gray cartoon represents the starting structure, and the orange cartoon is the structure averaged over the 83–112 ns interval. (H) Cartoon representation of TM3 and TM6 highlighting the kink in the TM6 that occurs in the 135–225 ns time interval (event 3). Orange and Magenta cartoons represent structures averaged over 83–112 ns and 290–350 ns, respectively. (I) Snapshots of TM3 and TM6 depicting positions of R3.50 and E6.30 residues and the distance between them and illustrating the movement of TM6 away from TM3 (event 5). Color code is the same as in panel G. (J) Detailed dynamics in the toggle switch W6.48. Evolution of the χ_1 and χ_2 angles is shown during the 140–146 ns time-interval when the toggle switch flips. Also shown are the snapshots at 0 ns and 143 ns time-points of the 5-HT and W6.48 (in spheres and colored by atom type, 5-HT in orange, and W6.48 in grey and cyan at 0 ns and 143 ns, respectively.).

doi:10.1371/journal.pcbi.1002473.g003

NPxxY sequence has been suggested to modulate the transition to the active state in the serotonin 2C receptor (5-HT_{2C}R) [24], and structural data show that the pi-pi interaction between 7.53 and 7.60 (Figure 1A) seen in inactive structures, is disrupted in active structures of β₂AR stabilized by nanobody [23], or complexed with the Gs heterotrimer [25]. In addition, the C_α distances between 7.53 and 7.60 in these active structures are larger (9.6 ???) than those in inactive ones (6.3 ???). The opening of the TM7-H8 angle is consistent with the transition to activated states of other GPCRs [22], and here we find that, in the 5-HT-bound 5-HT_{2A}R, H8 moves away from TM7 and the distance between the C_α atoms of Y7.53 and Y7.60 increases from ~6.2 ??? during the first 50 ns, to a value of 8 Å that remains stable for the remainder of the trajectory (Figure 3F).

Taken together, this sequence of steps observed in our simulations of 5-HT_{2A}R in complex with 5-HT (Figure 1B) not only captures structural effects of agonist binding on the status of the SM/FMs, but also provides a

mechanistically understandable hypothesis for this ordered sequence of apparently interrelated conformational changes that bring the 5-HT-bound 5-HT_{2A}R in line with known features of the activated state.

Significant differences are evident in the dynamics of the same SM/FMs in 5-HT_{2A}R bound to either the partial agonist LSD or the inverse agonist KET

Comparison of results in Figure 4 with Figure 3 brings to light the differences among the dynamic mechanisms connected with the binding of the three different ligands to the 5-HT_{2A}R, as detailed below.

KET bound to the 5-HT_{2A}R. In the KET simulation, the initially open ionic lock closes around 200 ns, and remains closed for the remainder of the trajectory, as the C_α distance between R3.50 and E6.30 residues stabilizes below 9 Å (Figure 4D, right panel), i.e., at a value consistent with inactive conformations of

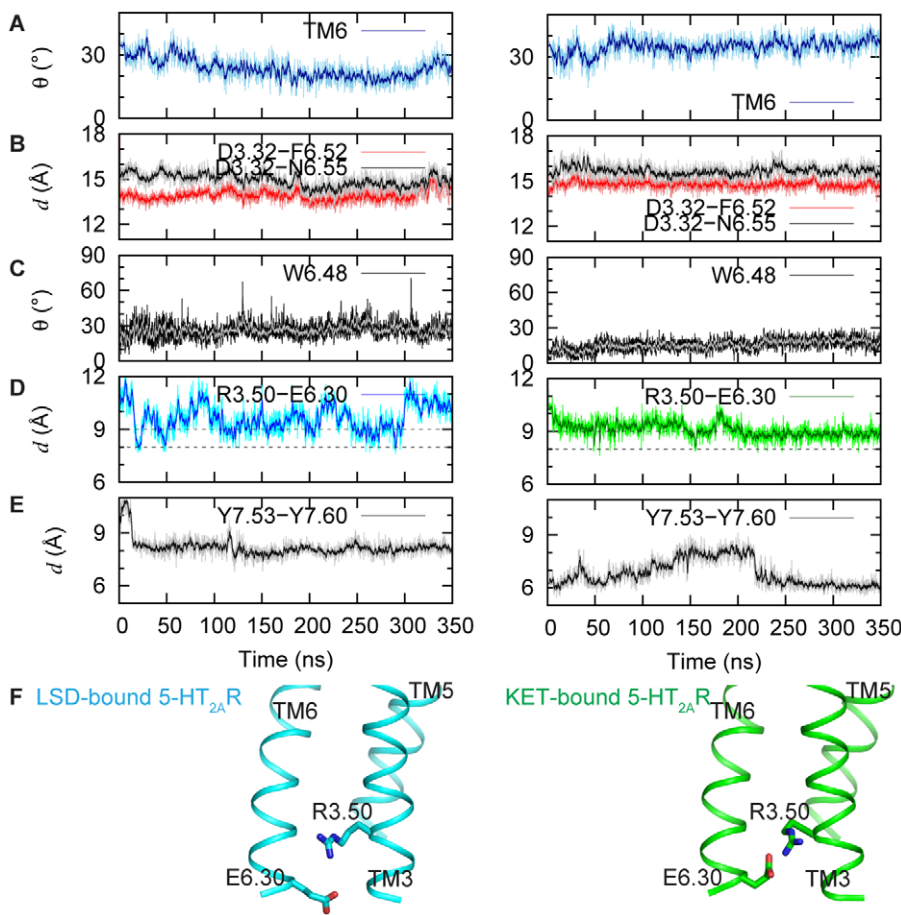


Figure 4. Dynamics of activation elements in LSD- and KET-bound 5-HT_{2A}R. (A–E) Left and right panels show the evolution of active state components in the 5-HT_{2A}R complexed with LSD and KET, respectively (for details see Figure 3). (F) Cartoon representation of TM3 and TM6 in the structures averaged over the last 100 ns of the LSD (cyan) and KET (green) trajectories, showing positions of R3.50 and E6.30 residues (in sticks). doi:10.1371/journal.pcbi.1002473.g004

cognate GPCRs [40]. Similarly consistent with a preference for this SM/FM in an inactive form of the receptor, is the observation in KET-bound 5-HT_{2A}R that neither the bend angle in TM6 (Figure 4A, right panel), nor the rotamer status of W6.48 (Figure 4C, right panel), change as they were seen to do in the trajectory of the 5-HT-bound receptor (Figure 3A, 3C). Thus, TM6 is more kinked with KET in the binding site than with 5-HT bound in the 5-HT_{2A}R, but no movement of the EC end of TM6 is observed relative to TM3 (Figure 4B, right panel). This is in sharp contrast to the behavior of 5-HT-bound receptor (Figure 3B), where significant changes in these activation elements were observed. Further, the dynamics of the NPxxY motif is also different in the KET-bound receptor, with the TM7-H8 pair maintaining a tighter conformation, and the Y7.53-Y7.60 C_α distance stabilized at ~6 Å for the later part of the trajectory (Figure 4E), i.e., 2 Å shorter than that in 5-HT_{2A}R complexed with 5-HT (Figure 3F). Note that such close proximity of the Y7.53 and Y7.60 residues has been suggested as a characteristic of an inactive state in GPCRs [41].

To validate the inferences from the KET simulation, and verify the distinctions between the agonist-bound and inverse-agonist bound forms of the 5-HT_{2A}R, we tested whether the binding of the inverse agonist KET would reverse the effect of the full agonist 5-HT on the conformational state of the serotonin receptor. To this end, we used the 5-HT-bound 5-HT_{2A}R structure (from the

average over the 300–350 ns trajectory interval of the simulation) as a starting structure for a new 500 ns simulation in which KET was substituted for the 5-HT (termed, KET-substituted, see Methods). As illustrated in Figure 5A, at ~240 ns into this new trajectory, the ionic lock that had opened in the agonist-bound simulation started to close when KET replaced it (the E6.30–R3.50 C_α distance decreased below 9 Å), and D3.49 and R3.50 formed a salt-bridged H-bond. Furthermore, from the same time point onwards, the structure of the TM bundle gradually became more similar to that stabilized by KET (the backbone TM RMSD relative to the KET-stabilized structure decreased by ~0.5 Å; Figure 5A).

These results show that the SM/FMs in the 5-HT_{2A}R bound to KET adopt characteristics observed in inactive GPCR states, which differ significantly from the ones observed with 5-HT in the binding site. This observation is in line with the opposite pharmacological properties of these two ligands.

LSD bound to the 5-HT_{2A}R. As shown in Figure 4 (left panel), the dynamic behavior of the LSD-bound receptor is in line with the pharmacological efficacy of LSD as a partial agonist, i.e., intermediate between those observed for the 5-HT- and KET-bound 5-HT_{2A}R constructs. Thus, in the LSD-bound receptor the ionic lock transitions between open and closed conformations (Figure 4D, left panel), as the R3.50–E6.30 distance fluctuates in the range of values proposed [40] for open (>9 Å) and closed (<9 Å)

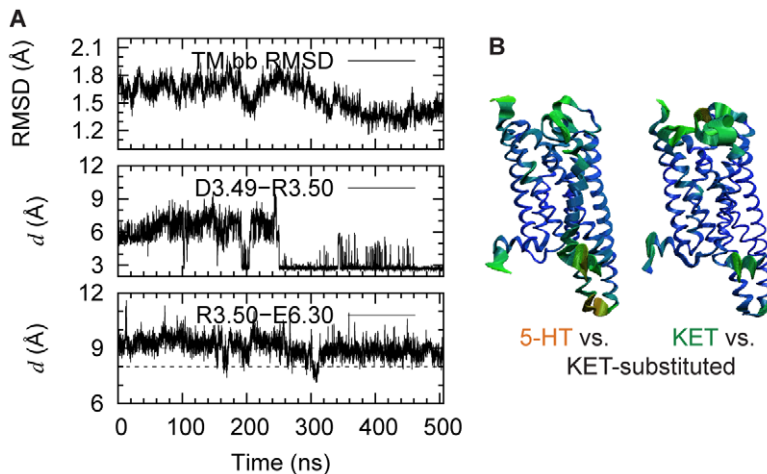


Figure 5. Characteristic dynamics of 5-HT_{2A}R induced by 5-HT are reversed by KET. (A) Evolution of the TM backbone RMSD of KET-substituted receptor compared to KET-bound receptor, averaged along 250–350 ns (top), the minimum distance between the carboxylate oxygens of D3.49 and the guanidine nitrogens of R3.50 (middle), as well as the C_x distance between R3.50 and E6.30 (bottom). (B) Extreme projections along the first eigenvector from Comb-ED analysis of the combined 5-HT-bound and KET-substituted receptors (left panel), as well as KET-bound and KET-substituted (right panel) trajectories. The receptor is shown in tubes, and colors depict magnitudes of conformational changes from small to large (from blue to green, and to red).

doi:10.1371/journal.pcbi.1002473.g005

ionic lock states. In the NPxxY motif region, the Y7.53–Y7.60 distance in the LSD-bound receptor remains in the range associated with an open conformation throughout the trajectory, similar to that in the 5-HT bound receptor (*cf.* Figures 3F and 4E). The bend angle around P6.50 in the LSD-bound receptor decreases from 35° to 15° (Figure 4A, *left panel*) with the EC end of TM6 bending towards the center of the protein bundle. However, the extracellular segment of TM6 does not come as close to TM3 as it does in the 5-HT simulation (*cf.* D3.32–F6.52 and D3.32–N6.55 in Figure 3B and Figure 4B, *left panel*).

Consistent with the incomplete opening of the ionic lock, the time-trace of the tilt angle of the W6.48 aromatic ring in LSD trajectory (Figure 4C, *left panel*) indicates as well that the dynamics of the toggle switch is intermediate: the complete flipping of W6.48, observed in the 5-HT simulation (Figures 3C, 3J), is replaced here by significant fluctuations in W6.48 orientation compared to the KET-bound 5-HT_{2A}R (Figure 4C, *right panel*). *Thus, in monitoring the steps in the dynamic sequence we find for the partial agonist LSD a series of intermediate dynamic modes that turn on the SM/FM forms associated with an active conformation, but not necessarily all of them together (e.g., the TM7-H8 angle is wider, and the ionic lock is broken, but with a fluctuating, not flipped W6.48).* Like the other two ligand types, the pattern generated by LSD is entirely consistent with its known pharmacological property.

The 5-HT_{2A}R in complex with either 5-HT, LSD, or KET visits distinct conformational spaces

The nature of similarities and differences observed in the dynamics of the 5-HT_{2A}R when it binds each of the three ligands was further evaluated with Combined Essential Dynamics (Comb-ED, see Methods) [42] performed on concatenated trajectories for 5-HT&LSD, 5-HT&KET, and LSD&KET, each combining the last 100 ns of the individual trajectories for the pair. The comparison of such combined trajectories by their projection along their first and second eigenvectors is shown in Figure 6A, which illustrates the differences in the conformational spaces sampled by the 5-HT_{2A}R bound to different ligands. Clearly, along the first eigenvector, the conformational spaces sampled by

the 5-HT-bound and LSD-bound receptor are seen to be more similar to each other than either one is to the space sampled by KET-bound 5-HT_{2A}R (note that the first and second eigenvectors are different in each plot because the concatenated trajectories differ, so that the sampled spaces shown in the plots for any one ligand-bound receptor appear at different positions).

The comparison in Figure 6B–C shows the differences in a structural context by indicating where the largest differences occur, as monitored by the magnitudes of the projections on the first eigenvectors (color coded from red, green to blue representing magnitudes from large, median to small, respectively). Also evident in this figure is the greater similarity between the dynamics of the 5-HT and LSD-bound receptors (Figure 6B–C, *top panel*). Comb-ED analysis identifies only insignificant differences between the agonist- vs. partial agonist-bound states of the receptor, with some variations in the positioning of the juxta-membrane H8 and in TM4 (Figure 6B–C, *top panel*). However, the structure of 5-HT_{2A}R in complex with either 5-HT or LSD is clearly distinct from that with KET bound, as seen in Figure 6B–C where the Comb-ED detects differences in TM5–6 (linked by IL3) and TM4 in the 5-HT vs. KET comparison (*middle panel*), and LSD vs. KET (*bottom panel*).

Differences between 5-HT_{2A}R complexes with the inverse agonist, and those with the agonists 5-HT or LSD, are apparent as well for TM1, TM3 and H8 (Figure 6B–C, *middle and bottom panels*). Thus, in the KET-bound receptor, Comb-ED identifies the movement of TM5 and TM6 toward TM3 at the IC end, consistent with the observed closing of the ionic lock in the inverse agonist state (Figure 4D,F, *right panel*). Furthermore, differences are evident at the EC end of TM6 between KET- and 5-HT-induced conformations, in agreement with the different level of kink in TM6 around the P6.50 in the two systems (compare Figures 3A and 4A). In addition, in line with the observed differences in the dynamics of NPxxY motif (Figures 3F and 4E), the Comb-ED analysis in the KET-bound receptor detects the motion of H8 toward TM7 to close the angle between them, consistent with earlier studies of cognate GPCRs [22,37,43].

Based on the Comb-ED results suggesting structural differences as well in TM1 and TM4 between the states of 5-HT_{2A}R

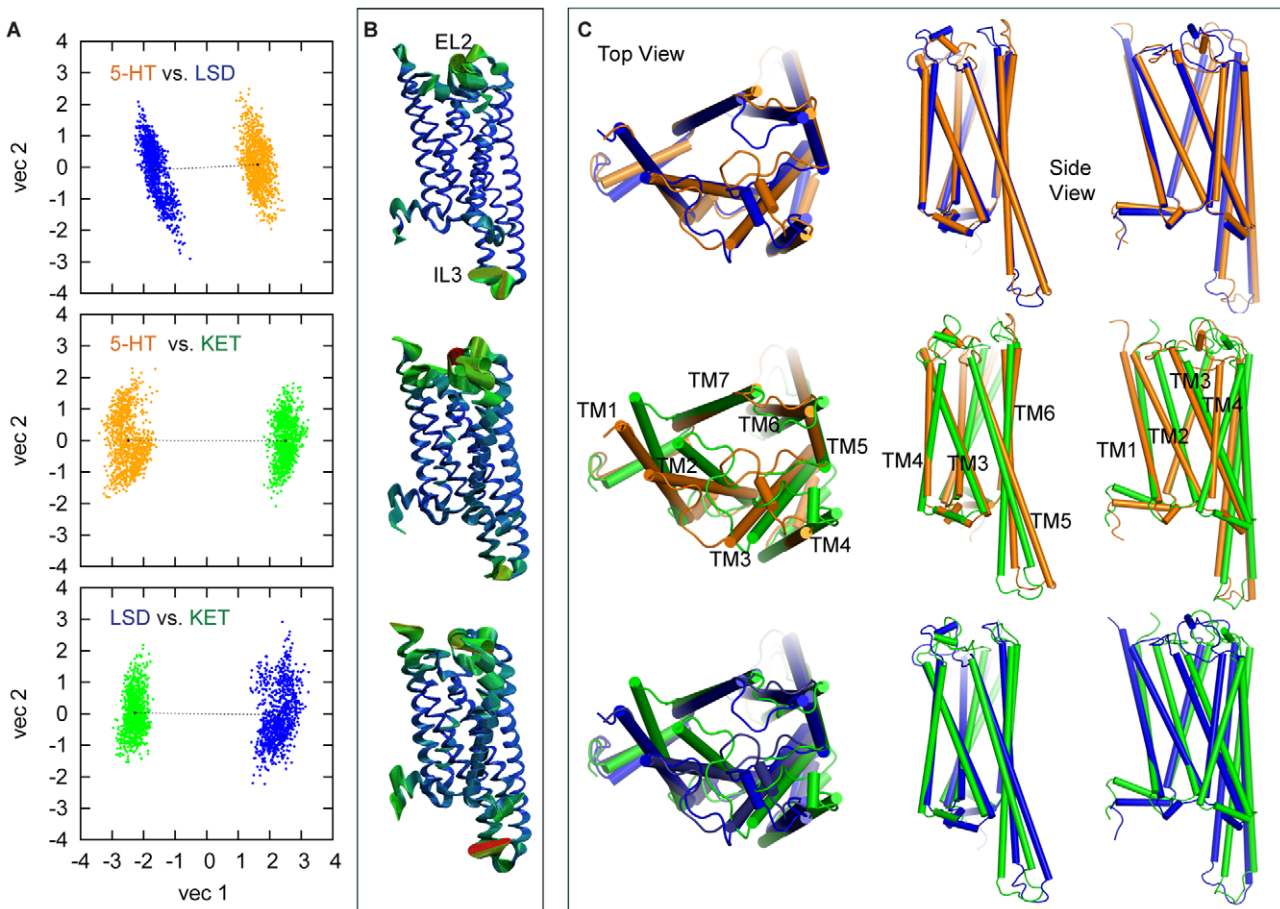


Figure 6. Comb-ED analysis of the conformational spaces visited by 5-HT_{2A}R bound to 5-HT, LSD and KET. (A) Projections along the first and second eigenvectors obtained from the Comb-ED analysis on the concatenated 5-HT-LSD (upper panel), 5-HT-KET (middle panel), and LSD-KET (lower panel) trajectories. The centers of the conformational space sampled by ligands are in black dots and are connected by black dotted lines. (B) Extreme projections along the first eigenvector of the combined 5-HT-LSD (top panel), 5-HT-KET (middle panel) and LSD-KET (bottom panel) trajectories. The receptor is rendered and colored as in Figure 5B. (C) Comparison of the 5-HT_{2A}R structures in complex with 5-HT, LSD or KET averaged over the final 100 ns aligned with seven most conserved residues in each TM [18]. The receptor structures in complex with different ligands are shown in cartoon and are colored as in panel A.

doi:10.1371/journal.pcbi.1002473.g006

stabilized by the three ligands (Figure 6B–C), we found different levels of tilt in TM1 and TM4 in the three states of the receptor. Thus, in 5-HT, LSD, and KET trajectories TM4 forms angles of 12°, 16° and 22°, respectively, with the membrane normal z axis; TM1 tilts so that in KET-bound compared to 5-HT-bound receptors its EC end is 3 Å closer to TM7 and its IC side is 1.5 Å farther from TM7. The differences in conformational changes of TM1 are consistent with the available X-ray structures of the activated GPCR, where a repositioning of the IC end of TM7 towards TM1 is reported in active β_2 AR [23] and opsin structures [20,21]. As discussed below, these tilt differences in TM1 and TM4 are reflected in the response of the membrane to the interaction with the protein, and thereby can affect the ligand-regulated oligomerization of the 5-HT_{2A}R.

The nature of the changes occurring in the transition from the “activated” 5-HT-bound state of the receptor, to the KET-bound “inactivated” state, is evidenced by the application of Comb-ED analysis to combined trajectories involving the KET-substituted simulation (started from an equilibrated 5-HT-bound receptor) (Figure 5B). Separately, two Comb-ED analysis were performed: One comparing the last 100 ns from the KET-substituted and the original KET-bound simulations, and the other comparing the

KET-substituted and the 5-HT-bound simulation. The projections along the first eigenvector of these combined trajectories (Figure 5B) reveal the internal consistency of the results and show that, upon KET substitution, the 5-HT_{2A}R structure deviated from the 5-HT-stabilized conformation and became similar to that stabilized by KET in our earlier simulation, with TM4 and TM6 helices changing the most. Consistent with the results in Figure 6, in the KET-substituted simulation the IC end of TM6 moved towards TM3, and TM4 became tilted.

In addition to Comb-ED analysis of pair-wise concatenated trajectories, we applied Comb-ED as well to all four trajectories (5-HT, LSD, KET, KET-substituted) concatenated together. The results (Figure S3 in Text S1) clearly show that KET-substitution transitions the receptor from the conformational states visited by 5-HT to those most visited when KET is bound in the receptor.

Ligand-dependent conformational changes in the receptor elicit corresponding structural re-arrangements in the surrounding lipid membrane

From the results of the comparative simulations we have identified two mechanisms of membrane re-organization in

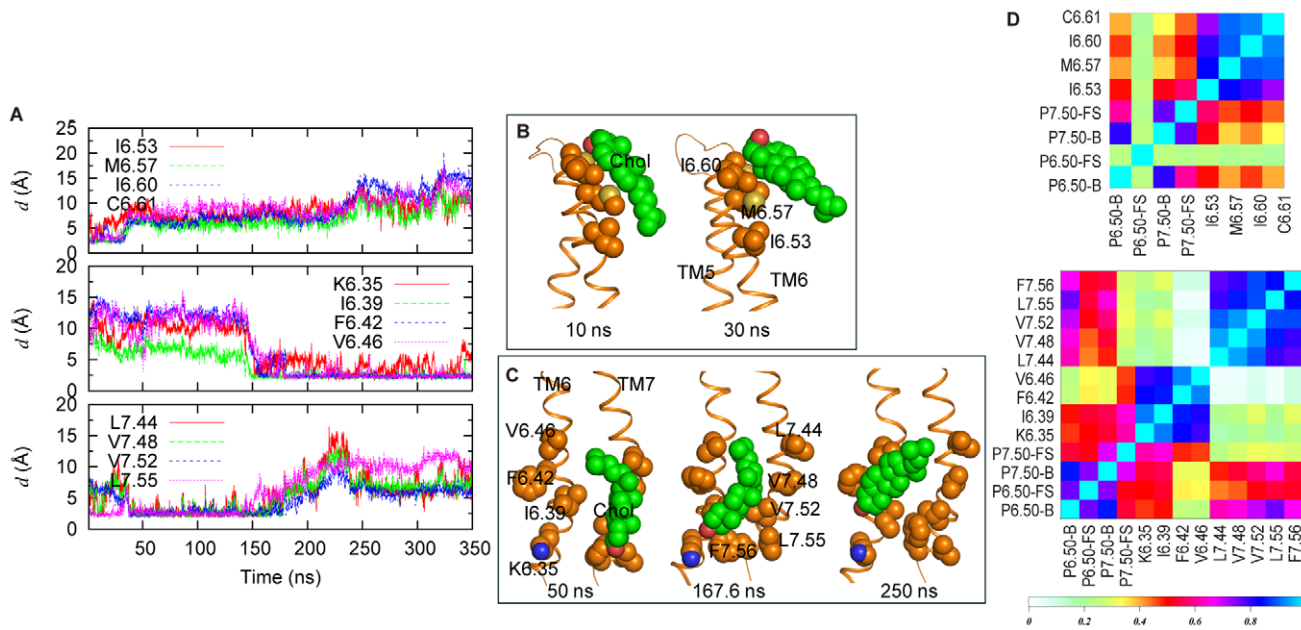


Figure 7. Cholesterol dynamics correlates with the structural transitions in agonist-bound 5-HT_{2A}R. (A) Evolution of the minimum distances between the Chol at the EC end of TM6 and selected TM6 residues in the 5-HT simulation (top panel). Time traces of the minimum distances between the Chol at the IC ends of TM6–7 and selected residues on TM6 and 7 (middle and bottom panels). The Chol initially in contact with the L7.44, V7.48, V7.52, and L7.55 residues on TM7 moves towards TM6 and engages in interactions with the residues K6.35, I6.39, F6.42, and V6.46 on TM6. (B) Snapshots at 10 and 30 ns showing the Chol from the top panel of (A) interacting with EC TM6. (C) Snapshots at 50, 167.6 and 250 ns showing the Chol from the bottom panels of (A) interacting with either IC TM6 or IC TM7. (D) Matrix of Pearson's score tests performed on the dynamics quantities presented in the top panel of (A) and on the bend ("B") and face-shift ("FS") angles around P6.50 and P7.50 (top panel). Matrix of Pearson's score tests performed on the dynamic quantities presented in middle and bottom panels of (A) and on the bend ("B"), and face-shift ("FS") angles of P6.50 and P7.50 (bottom panel).

doi:10.1371/journal.pcbi.1002473.g007

response to the conformational changes associated with the dynamics of the ligand-bound receptor: (i)-the direct interactions of the receptor with the Cholesterol (Chol) constituent of the membrane, and (ii)-the deformation of the membrane around the GPCR, which modulates the local thickness of the bilayer and the hydrophobic mismatch that can drive oligomerization of the 5-HT_{2A}R [32].

Cholesterol interacts with the structural elements of GPCR activation. Cholesterol has been implicated in GPCR function and activation [44] and shown to bind to preferred sites of rhodopsin in extended simulations of this GPCR in lipid membranes [43]. Here we found that the regions ranked highest in Chol population during the simulation of the 5-HT_{2A}R were the IC end of a TM bundle including TMs 1, 2 and 4; the EC ends of TMs 2 and 3; and the EC and IC ends of TMs 6 and 7 (see Table S1 in Text S1). Notably, these sites were also found to be the areas of high Chol-density in earlier studies on rhodopsin [43,45,46], as well as in a 250 ns simulation of rhodopsin in a membrane with the same lipid composition as used here (SDPC/POPC/Chol - see [32]). We hypothesized, therefore, that Chol binding at these preferred locations may have some functional importance observable through effects on the monitored SM/FMs. Given the prominent structural changes in TM6 observed in our simulations of the 5-HT-bound 5-HT_{2A}R, this hypothesis was investigated for Chol at the IC and EC ends of TMs 6 and 7.

Figure 7 summarizes Chol dynamics around the EC and IC ends of TMs 6 and 7, and its relation to the activation elements in 5-HT-bound receptor. The Chol at the EC end of TM6 is seen to be in direct contact with residues M6.57, I6.60, and C6.61 at the initial stages of the simulation (Figure 7A, upper panel), and to move away from these residues within the first 40 ns (Figure 7B).

Interestingly, during the same time interval, we observe changes in one of the identified SM/FMs, as TM6 straightens out at the EC end, and starts moving towards TM3 (cf. Figures 2–3). Near the 140 ns time-point, another Chol, initially in contact with the IC end of TM7, moves towards TM6 and establishes interactions with residues K6.35, I6.39, F6.42 and V6.46 (Figure 7A, middle and lower panels, and Figure 7C). Remarkably, this shift of Chol away from TM7 and toward TM6 coincides with the time when the toggle switch W6.48 flips (Figures 2–3), and TM6 starts to bend away from TM3 at the IC end (Figures 2–3). Thus, the time dependence of Chol dynamics at the IC and EC ends of TM6 suggests its participation in the development of the activated conformation in the agonist-bound 5-HT_{2A}R.

To quantify the apparent correlation between the Chol dynamics and the structural changes in the 5-HT/5-HT_{2A}R simulation we calculated the Pearson correlation coefficients between the dynamic quantities presented in Figures 3 and 7, and constructed the matrix of the corresponding Pearson R^2 scores following a protocol described earlier [43]. The strong correlation between Chol-TM6 distances and agonist-induced changes in 5-HT_{2A}R is evident from the high values of the correlation coefficients (Figure 7D) calculated for the MD trajectory.

Notably, the pattern of Chol-GPCR interactions around TM6 in the 5-HT/5-HT_{2A}R trajectory is different from those observed in either the LSD-bound or the KET-bound receptor. For example, analysis of the KET simulation shows a single Chol around the IC ends of TM5 and TM6 (Table S1 and Figure S4 in Text S1). This Chol molecule is engaged in interactions with F6.42 and V6.46, the same two residues of TM6 that we found to interact as well with Chol in the 5-HT trajectory (see Figure 7). But in contrast to the 5-HT simulation, the cholesterol positioned near

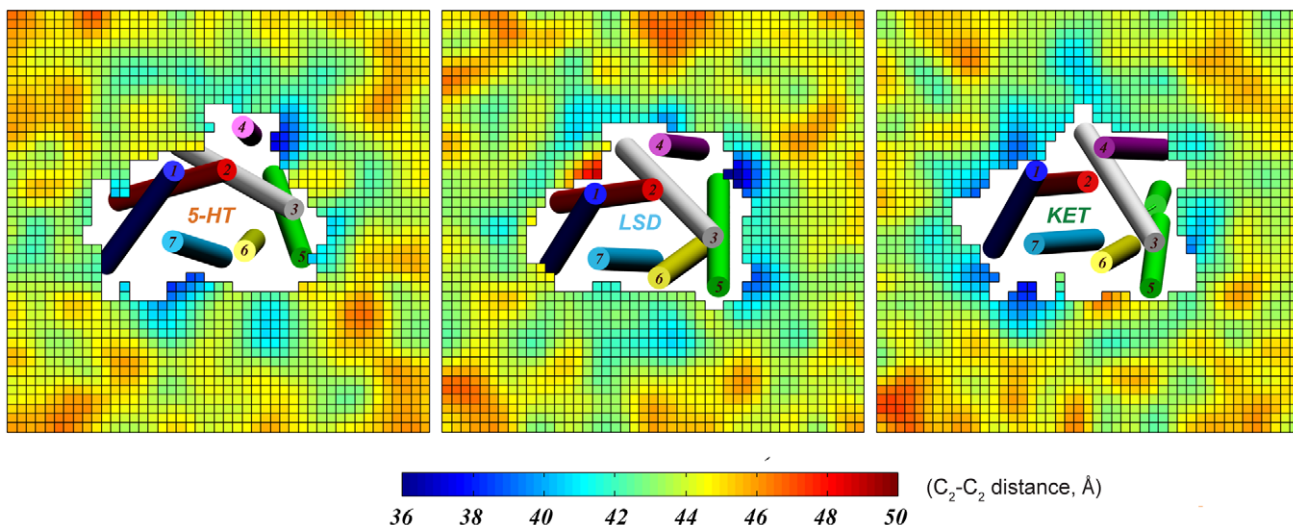


Figure 8. Hydrophobic thickness profiles of simulated membranes around 5-HT_{2A}R in complex with 5-HT, LSD, or KET. The structures of the various ligand-bound receptor structures averaged over the last 100 ns of the simulations are shown in cartoon, with only the helices depicted (in different colors) with corresponding TM numbers. The colored fields represent distances (in Å) between lipid backbone C₂ atoms from the opposing leaflets. For this analysis, for each simulated system the membrane plane was divided into square 2 Å × 2 Å bins, and the average C₂-C₂ distances in each bin were collected by scanning the last 100 ns of trajectory.

doi:10.1371/journal.pcbi.1002473.g008

the IC end of TM6 in the KET trajectory is also in contact with residues from TM5: F5.59 and I5.62. The specificity of these interactions is suggested by the observation that in the KET-substitution simulation (initiated from the 5-HT-induced conformation of the receptor), Chol interactions rearrange to the pattern observed in the regular KET simulation. Thus, in the KET-substitution simulation Chol still interacts initially with F6.42, V6.46, and I6.39, but when the ionic lock starts to form, F6.42 flips (without loosing contact with the cholesterol) towards TM5 and establishes stable interactions with F5.59 that brings TM5 and TM6 helices together from the IC side. Similarly, in the KET simulation, cholesterol near TM5 and TM6 appears as well to bring these two helices together by forming a bridge between F6.42 and F5.59.

When considered together with the ionic lock data (Figure 4), these results suggest an active involvement of cholesterol near the IC end of TM6 in establishing differential ligand-induced conformational dynamics of the receptor.

Membrane shape exhibits distinct patterns in response to the 5-HT_{2A}R conformations attained by pharmacologically different ligands

The distinct conformational changes in the receptor produced by the binding of the different ligands (see above) produce different patterns of bilayer deformations around the receptor protein in complex with the different ligands (Figure 8). This difference is a result of the tendency of the lipids to minimize the hydrophobic mismatch at various TMs, i.e., the difference in the hydrophobic lengths presented to the membrane by the corresponding TMs in the different receptor complexes (see detailed discussion in [32]). Therefore, hydrophobic thickness profiles of membranes around 5-HT_{2A}R in the simulated complexes with 5-HT, LSD, and KET, shown in Figure 8, reveal remarkable differences in the membrane organization around individual TMs in the three systems. For example, the membrane appears thinner around TM4 and TM6 in 5-HT (left panel) than in the KET simulation (right panel), whereas at TM1 the bilayer is thicker in the LSD (middle panel) than in the complexes with 5-HT or the KET.

We have developed a quantitative method (CTMD), for the analysis of such membrane deformations and the significant residual exposure to unfavorable hydrophobic-hydrophilic interactions at specific TMs that results from an incomplete alleviation of the hydrophobic mismatch [32]. When applied to the 5-HT_{2A}R complexes discussed here, residual exposure [32] was found at TM4 for all three complexes, although the values were different possibly because the TM4 tilt is different in the KET, LSD and 5-HT trajectories (see above). Because the extent of the hydrophobic mismatch around the TM helices is considered to be a driving force for oligomerization [32,47,48], we had compared the residual exposure energies at all TMs in the simulation results for the three complexes. At TM1 it was found to be substantial only in the KET simulation, consistent with the conformational changes we observed for TM1 in different systems (see above), and at TM5 it appeared to be relatively similar in all three complexes, but somewhat more pronounced in the 5-HT-bound structure; lastly, the residual exposure at TM6 is largest as well in the 5-HT trajectory, possibly due to the relatively straighter configuration of this helix in the 5-HT simulation (Figures 3–4). One possible mechanism to reduce the energy penalty for this residual exposure in the membrane-embedded receptor conformation produced by the binding of a particular ligand, is to bring together the TM domains where the residual exposure is largest. Therefore, we proposed [32] that this represents a membrane-determined energy drive for the association of the proteins in the membrane.

Consequently, our data in Table 2 of [32] suggests that if the hydrophobic mismatch is the driving force for receptor oligomerization, then the contact interfaces for oligomerization of the 5-HT_{2A}R will be different in the complexes with 5-HT, LSD, or KET. According to this mechanism, ligands will not only regulate the extent of GPCR oligomerization, but will also influence which TM domains constitute the oligomerization interface. Thus, a comparison of residual surface area values at different TMs in 5-HT, LSD, and KET simulations implicates TM1, TM4 and TM5 as likely participants in the oligomerization interface of 5-HT_{2A}R in complex with KET, TM4 and TM5 in the oligomerization interface of LSD-bound receptors, and TM5 (and possibly TM6,

TM4 and TM2 as well) as the most likely participants in the oligomerization of 5-HT-bound serotonin receptor.

In addition, the results in Table 2 of [32] for the 5-HT and KET simulations imply that overall the inverse agonist KET will promote more extensive hydrophobic mismatch-driven oligomerization, since the residual surface area value summed over all TMs is about 90 Å² higher for KET-bound 5-HT_{2A}R than it is for 5-HT-bound receptor. This prediction is in excellent agreement with the experimental data on ligand-regulated oligomerization on β₂AR [31], where in comparison to the agonist isoproterenol, the binding of an inverse agonist was suggested to promote tighter packing on β₂AR protomers and/or to result in formation of higher-order oligomeric structures.

With regard to the validation of the ligand-dependent dynamic properties, it is important to note that similar residual exposure is observed in the two KET-bound simulations starting from very different initial conformations. Thus, the trend of large residual exposures at TM1, TM4, and TM5 of the KET system is also observed in the KET-substituted system (Table S3 in Text S1). Moreover, near the TMs where the hydrophobic mismatch is alleviated by the membrane remodeling (e.g., TM6), the membrane has similar thickness in both the KET and KET-substituted system (Figure S6 in Text S1).

Discussion

The MD simulations of the 5-HT-, LSD- and KET-bound 5-HT_{2A}R reported here provide the first molecular representation of the different effects that pharmacologically distinct ligands can have on the 5-HT_{2A}R. The concepts of “functional selectivity” [49,50] and “receptor bias” [51] are frequently being used to explain the increasingly common observation of differential responses elicited by different ligands from the same receptor (e.g., for 5-HT_{2A}R see [4,52]). However, no structural context had been identified for the distinct effects on the dynamics produced in the same GPCR by the binding of pharmacologically different ligands. Here we simulated the dynamics of the 5-HT_{2A}R binding of such pharmacologically distinct ligands, and identified different effects on the SM/FMs of the receptor. These effects were shown to lead to different rearrangements that correspond to the different levels of activation known to be produced by these ligands. Notably, the differential effects were shown to be consonant with the pharmacological characterization of the three ligands as a full, partial and inverse agonist, respectively. To our knowledge, such inferences were obtained for the first time here from unbiased atomic MD simulations, but they are in line with the increasingly detailed experimental evidence about ligand-related functional selectivity [49,50,51,53,54,55,56,57,58,59,60,61,62,63,64,65,66], with the proposals of ligand-selective conformations in the 5-HT_{2A}R [67] and the D₂R [68], and with structural data indicating that GPCRs such as β₂AR are stabilized in distinct conformational states by inverse, partial, or full agonists - respectively [12,13].

In the current simulations, structural changes associated with SM/FM characteristics of an “activated state” of the 5-HT_{2A}R appear in sub-microsecond trajectories. In contrast, experimentally determined GPCR activation timescales generally vary from microseconds (photoactivation of rhodopsin [69]) to seconds (β₂AR in living cells [70]). We emphasize that the conclusions reached here do not require the simulations to have converged to an “active state structure” of the kind claimed for the constructs determined crystallographically. Indeed, a number of modes of activation proposed from experiment share this characteristic and can also be significantly faster [71,72,73]. But in general, there are many reasons for the time scale differences between our results

and functional measurements. In particular, the simulated system is an idealized construct in that all interaction components are placed in optimal positions to be at or near their targets. Titratable groups are also assigned their final charge states, e.g., when the D3.49 and E6.30 are in the protonated form in some of the constructs. Interestingly, the specific protonation form does not determine whether the ionic lock is formed or not (see Figures 3–4, and Figure S5 in Text S1); rather, the determinant factor is seen from our results to be the nature of the dynamics induced by the binding of a specific ligand. But considering that inactive GPCR (β₂AR) may be pre-coupled to G-protein Gs [31] and the protonation of E3.49 in rhodopsin (an activation step) depends on transducin [74], the degree of precoupling will likely play a role in the activation time. Moreover, the simulation conditions (such as pH, salt, lipid composition, and crowding) certainly do not mimic completely those surrounding the receptor in living cells (e.g., it is known that the highly flexible DHA chain of SDPC, included in the lipid mixture used here, facilitates GPCR activation [75]), and similar time-scale differences have been observed between computer simulations and experiments for other GPCRs [76,77].

The response of the membrane environment to the different ligand-induced structural re-arrangements produces a reorganization of the membrane around the receptor. This is reflected in **(i)**-the involvement of Chol in direct interactions with the protein [43,78], that was shown here to affect the dynamics of the SM/FMs, and **(ii)**-the membrane deformations around the TM bundle of a GPCR [48,79], described here with the use of the CTMD method [32]. Because the different ligand-determined conformational changes in 5-HT_{2A}R establish different patterns of local perturbations in membrane structure around the receptor complex, they were suggested to promote different ligand-dependent receptor oligomerization patterns through the hydrophobic mismatch between the TMs and the surrounding membrane [32]. This is supported by observations in the literature that: **(i)**- oligomeric associations of the dopamine D₂R [27], 5-HT_{2C}R [28], and the β₂AR [31] is ligand-sensitive; and **(ii)**- GPCR self-assembly is regulated by the mismatch between the hydrophobic length of the TM segments of GPCRs and the hydrophobic thickness of the lipid bilayer, as suggested by both experimental results [80] and computational studies for rhodopsin [32,48,79]. Along these lines, the results presented here suggest that the dimerization interfaces of 5-HT_{2A}R oligomers will be different for inverse agonist-, partial agonist-, or agonist-bound complexes, and moreover that the inverse agonist KET would promote more extensive 5-HT_{2A}R oligomerization than the full agonist (5-HT). We note that these experimentally testable predictions regarding possible oligomerization interfaces were obtained by analyzing monomeric GPCRs in complex with different ligands, without the need to simulate the dimers or higher oligomers.

Methods

Construction of the simulated systems

Several model systems of the serotonin 5-HT_{2A}R receptor were studied with all-atom MD simulations in explicit models of the hydrated lipid membrane environment. The 5-HT_{2A}R was simulated in complex with three ligands known to exhibit different pharmacological efficacies: the full agonist 5-HT, the partial agonist LSD, and the inverse agonist KET (Figure 2A).

5-HT_{2A}R constructs. For the simulation of 5-HT bound 5-HT_{2A}R, the protein was modified twice, very slightly, in regions distal to the binding site and the SM/FMs. The original receptor construct had a specific truncation of IL3 so that it consisted of 296 residues, from H1.28 to D5.57 and from R6.21 to K7.73, with an

Ala-Ala linker between them (H1.28–D5.75–AA–R6.21–K7.73, where “–” denotes truncation). To match observations in crystallographic structures of several GPCRs [20,25,81], we thus added, at 112.5 ns, four residues to the IL3 (H1.28–L5.79–AA–S6.17–K7.73) in order to extend helical parts of TM5 and TM6, respectively, by two turns. The extension was done as follows: an average structure of the protein (including the ligand and palmitoyl derivative) was obtained from the trajectory between from 83.5 to 112.5 ns. The averaged structure was minimized first with constrained protein backbone and ligand heteroatoms followed by minimization without constraints. To enhance the flexibility of the truncated IL3, we extended the intracellular ends of TM5 and TM6 by 2 turns of helix each using Modeller [82], and selected the representative model by clustering the 100 models using either the extended TM5 or TM6. The loop between the extended TM5 and TM6 was refined using Modeller. The protein with extended TM5 and TM6 together with the ligand and palmitoyl chain was minimized first with protein backbone and 5-HT heteroatoms constrained, followed by complete minimization. The minimized complex was inserted in the lipid/water/ion environment from the snapshot at 112.5 ns to conserve interactions, after which the entire system was minimized and equilibrated with constraints on the protein backbone (velocities were reassigned in a random distribution based on the temperature). For the second extension, at 174.2 ns (i.e., 61.7 ns after extending TM5 and TM6), we added three more residues at the N-terminus (S1.25–L5.79–AA–S6.17–K7.73) to allow TM1 to reach beyond the lipid phosphate group region of the model membrane so as to avoid artificial interactions between the positive N-terminus and negative phosphate groups in membrane lipids. In addition, the N-terminus was acetylated and the C-terminus was N-Methylamidated to further avoid charge-charge interactions between termini and lipids. The simulations were then continued and the results reported here are from the 350 ns trajectory. Note that the initial homology model of 5-HT_{2A}R includes an artificially open “ionic lock” between residues R3.50 and E6.30 due to the use of the β_2 adrenergic receptor (β_2 AR) template in the homology modeling [83]. In the β_2 AR X-ray structure [45] the ionic lock is broken due to the co-crystallized lysozyme, but has been shown to consistently reform in MD simulations of inactive β_2 AR without the lysozyme [40].

The simulations of LSD-bound and KET-bound 5-HT_{2A}R, started from the same conformation as for the 5-HT bound 5-HT_{2A}R except that they included the extensions from the very beginning. In addition, to test whether KET, as an inverse agonist, is capable of reversing the conformation induced by the bound agonist 5-HT, we substituted 5-HT with KET in the activated 5-HT_{2A}R structure obtained at the end of the 5-HT simulation, and restarted that simulation with KET for an additional 500 ns (termed “KET-substituted simulation”). The protocol for this switch of ligand was as follows: (i) An average structure (protein+5HT+palmitoyl chain) was generated using the last 50 ns of 5-HT simulations, and then minimized; (ii) 5HT was substituted by KET so that the docking pose of KET (Figure 2D, left panel) is aligned with the minimized average structure using backbone atoms of binding site residues: D3.32, S3.36, S5.42 and S5.46. The complex (protein+KET+palmitoyl chain) was minimized by fixing the heteroatoms of KET and constraining backbone atoms of the protein; (iii) The minimized complex was combined with the lipid/water/ion environment from a snapshot at 350 ns of the 5-HT simulation, to conserve the interaction between the protein and the environment. Lipid/water/ion was minimized and then equilibrated. Finally the whole system was equilibrated by reducing constraints on protein backbone atoms

and KET heteroatoms. Velocities were reassigned based on the temperature.

Residues D3.49 and E6.30 were protonated in the 5-HT and LSD simulations (see also Discussion section, above), and deprotonated in the KET simulations (including KET-substituted simulation). We note that the protonation state of the E6.30 residue does not affect the state of the ionic lock, as we show in the separate simulation of KET-bound 5-HT_{2A}R where E6.30 residue is protonated (see Figure S5 in Text S1).

In all simulations, C7.70 was palmitoylated by moving the coordinates of the palmitoyl chain (PALM) from PDB 2RH1 [45] onto the C7.70 of 5-HT_{2A}R.

Loop structures determined from ab initio loop prediction. To enable full-scale 5-HT_{2A}R simulations, we refined the loops in 5-HT_{2A}R homology model described recently [83] using the Monte Carlo-Scaled Collective Variables *ab initio* method [84,85]. For details see Methods and Table S2 in Text S1.

Initial placement of the ligands. Protonated 5-HT, LSD and KET were docked into 5-HT_{2A}R using several docking protocols, including Autodock 4 [86], Simulated Annealing-Docking [87], Glide (Schrödinger Inc.), and IFD (Schrödinger Inc.). In Autodock, the GA-LS algorithm and a maximum number of 2.5×10^7 evaluations were used. Simulated Annealing-Docking was carried out following a protocol previously established in our lab [87,88] starting from a binding pose of 5-HT predicted by Autodock and consistent with experimental data. Glide [89] was carried out with and without H-bond constraints on D3.32 and/or S5.46. Applying H-bond constraints on S5.46 generated more docking poses that were consistent with the experimental data. IFD [90] was carried out starting either from scratch or from Glide docking poses that were consistent with experimental data. Other docking parameters were set to default values.

These procedures generated docking poses consistent with experimental data in the literature [2,6,7,91,92] (Figure 1A–D). In particular, for KET, IFD produced a cluster of docking poses in which the amines of the ligands interacted with D3.32 and S5.46, and its quinazoline ring immersed deep into the binding pocket close to W6.48. The binding site remained almost unchanged except that F6.52 rotated to avoid steric clashes with KET (Figure 1D). In this docking pose, which was used in the simulations, KET was in direct contact with the aromatic cluster (F5.47, F6.44, W6.48, F6.51 and F6.52) by forming an edge-to-face interaction with W6.48.

Internal waters. X-ray structures of several GPCRs show water networks around the toggle switch W6.48 and the NPxxY motif [45,93,94,95], and these are hypothesized to be important for receptor activation [96]. Internal waters were therefore introduced by solvating the 5-HT_{2A}R with Grand-Canonical Ensemble simulations using the Monte Carlo program MMC [97]. The procedure placed waters around W6.48 and the NPxxY motif consistent with the X-ray structures of cognate GPCRs.

Lipid membrane composition and protein-membrane complex preparation. The 5-HT_{2A}R-ligand complexes were embedded in identical mixed and hydrated 7:7:6 1-stearoyl-2-docosa-hexaenoyl-sn-Glycero-3-phosphocholine (SDPC)/phosphatidylcholine (POPC)/Chol membranes. The choice of the lipid mixture was dictated by several factors: (i) Chol is known to be important for modulating ligand binding, G-protein binding and activation of serotonin receptors [44], and has even been found in complex with the X-ray structures of amine GPCRs elucidated recently; (ii) POPC represents a typical phospholipid component of the bilayer membrane, with one saturated and one mono-unsaturated acyl chain; and (iii) SDPC lipid has been implicated specifically in the function of various

GPCRs [98] and is abundant in neuronal tissues. In addition, the use of this lipid composition enables a comparison of Chol dynamics around 5-HT_{2A}R with observations from earlier MD studies of rhodopsin in somewhat different Chol-containing mixed membranes [43].

The lipid bilayer model was generated using VMD [99] to construct first a 120 Å×120 Å (in the x-y plane) hydrated POPC membrane patch consisting of 406 lipids; then, half of the POPC lipids were transformed to SDPC by translating corresponding atoms, i.e., from the POPC headgroups to PCGL, from the 16:0 *sn*-1 chain to STEA, and from the 18:1 *sn*-2 tail to DHA (missing atoms were built using internal coordinates in the all-atom CHARMM27 force field [100] with CHARMM31b1 [101]). To reduce steric clashes between POPC and SDPC molecules, we made use of the relatively straight DHA chains from the equilibrated SDPC membrane bilayer (<http://www.lipid.wabash.edu/>), and replaced all the DHA chains in the current membrane patch with the straight DHAs. The 5-HT-, LSD-, or KET-bound 5-HT_{2A}R were inserted into the lipid matrix by aligning the backbone of its seven most conserved residues (one in each TM, see [18]) with those of rhodopsin immersed in a POPC membrane [22]. Lipids within 0.8 Å of the protein and PALM were then removed leaving 354 lipids in total. 26 SDPC and 26 POPC in each leaflet were randomly replaced with Chol (PDB 3D4S [46]), by fitting Chol's C4, C5 and C6 atoms to STEA's C5, C6 and C7 or POPC's C35, C36 and C37. Chol positions were then refined by lateral translation to avoid clashes with other Chol, SDPC or POPC lipids. Finally, the systems were solvated with TIP3 water and 0.15 M NaCl salt. The final simulated systems consisted of 125 SDPC, 125 POPC, 104 Chol and 20–22K water molecules resulting in a total of 106–114K atoms.

Force-fields and MD simulations

The parameters for 5-HT were taken from an earlier study [7]. For LSD and KET, the results of geometry optimization and electrostatic potentials obtained from quantum mechanical calculations with the Gaussian program (Gaussian, Inc., Wallingford, CT) were used as input to the Restrained-ElectroStatic-Potential fit method [102] implemented in Antechamber [103] to derive charges. CHARMM topology and parameter files were then prepared with Antechamber using Restrained-ElectroStatic-Potential charges and GAFF force field. Force field parameter files for 5-HT, LSD and KET are included in Text S1. For protein, PALM, lipids etc., the all-atom CHARMM27 force field with CMAP corrections [100] was utilized (this approach is similar to a procedure used successfully in previous studies [104,105]).

All MD simulations were performed with the NAnoscale Molecular Dynamics (NAMD) suite [106]. As established in similar studies in the lab (e.g., see [107]), the simulations were conducted under constant temperature and pressure conditions with anisotropic pressure coupling, and utilized PME for long-range electrostatics [108]. The Nose-Hoover Langevin piston method [106] was used to control the target pressure with the LangevinPistonPeriod set to 100 fs and LangevinPistonDecay set to 50 fs. All MD simulations were performed with rigidBonds allowing 2 fs time step.

All the simulated systems were equilibrated following a procedure described recently [109]. According to this protocol, the 5-HT_{2A}R backbones and the heavy atoms of the ligands were initially fixed and then harmonically constrained, and water was prevented from penetrating the protein-lipid interface. Constraints were released gradually in four 300 ps-step MD simulations with decreasing force constants of 1, 0.5, 0.1 and 0.01 kcal/(mol·Å²),

respectively. Following this equilibration phase, all three GPCR-membrane complexes were simulated for 350 ns.

The stability of the simulated complexes was monitored from the backbone RMSDs of the TMs in 5-HT_{2A}R using the following definitions for TMs: L1.29–L1.59, A2.38–Y2.67, L3.24–N3.56, S4.38–V4.62, D5.35–K5.67, N6.29–I6.60, G7.32–F7.56 and K7.58–I7.68. As illustrated in Figure 1E, after initial equilibration, the RMSDs in all the three systems were stable and fluctuated around or below 2 Å. In all three simulations the ligands maintained key interactions with the receptor (Figure 1B–E), consistent with previous experimental data [2,6,7,91,92].

Analysis of MD trajectories

To quantify the changes in protein structure produced by the simulations we used various analysis tools. Analysis of protein structural data was carried out with PTRAJ in AMBER 9 [110] and other tools discussed below. To quantify helix distortion parameters in the simulations, we used the Prokink package [111] implemented in Simulaids [112]. The correlation analysis on the time-dependent data of different variables, such as helix bend angles, face-shifts, as well as Chol-protein distances, was conducted following the procedure described in [43]. Briefly, the correlation analysis was carried out on two separate sets of dynamic variables. In the first, we followed the time-sequence of $m=8$ selected variables that included proline kink and face-shift angles in TM6 and TM7, the minimum distances between the Chol at the EC end of TM6 and the residues on TM6 (I6.53, M6.57, I6.60, C6.61). In the second set, $m=12$ dynamic variables were selected that included proline kink and face-shift angles in TM6 and TM7, the minimum distances between the Chol at the IC end of TM6–7 and the residues on TM6 and TM7 (K6.35, I6.39, F6.42, V6.46, L7.44, V7.48, V7.52, L7.55, F7.56).

For each set, we first studied pair-wise correlations between different variables, and constructed the matrix of coefficients of determination, R^2 (Figure 7D of the main text) using Spearman's rank correlation test (see for instance Ref. [113]). In this method, given N_{frames} pairs of observations, (x_i, y_i) , first the x_i and y_i values separately are assigned a rank, and then the corresponding difference, d_i between the x_i and y_i ranks is found for each pair. The R^2 is then defined as:

$$R^2 = \left(\sum_{i=1}^{N_{\text{frames}}} d_i^2 \right)^2 \quad (1)$$

Because it uses rankings, Spearman's method eliminates the sensitivity of the correlation test to the function linking the pairs of values and thus is preferred over parametric tests when no *a priori* knowledge exists on the functional relationship between x_i and y_i pairs.

Combined Essential Dynamics (Comb-ED) analysis

To compare the conformational spaces of 5-HT_{2A}R stabilized by the different ligands (i.e., 5-HT, LSD and KET), a Combined Essential Dynamics analysis [42,114] was performed on C_α atoms of the protein using Gromacs 3.3 [115]. Essential dynamics analysis separates the configurational space into an essential subspace with a few degrees of freedom which describe overall motions of the protein that are likely to be relevant to its function, and a physically constrained subspace describing local fluctuations. The method is based on the diagonalization of the covariance matrix of atomic fluctuations defined by:

$$C_{ij} = \langle (x_i - \langle x_i \rangle)(x_j - \langle x_j \rangle) \rangle \quad (2)$$

where x_i are the three Cartesian coordinates of the carbon atoms C _{α} of the molecule under study, and the angular brackets denote averages over an ensemble of configurations and over the simulation time. The diagonalization of Eq. (3) yields eigenvectors that describe the directions of correlated positional changes in the molecule, whereas the eigenvalues indicate the total mean square fluctuation along these directions.

In the Comb-ED, the covariance matrix is calculated for two or more concatenated trajectories, which are fitted on the same reference structure. Given this construct, the eigenvectors resulting from Comb-ED do not represent the essential degrees of motion of the molecules, but rather reveal differences and/or similarities in the dynamical and structural characteristics of the compared simulated structures. To identify structural differences between 5-HT_{2A}R stabilized by the three ligands, Comb-ED analysis was performed on 3 concatenated trajectories obtained by combining the trajectories for the pairs 5-HT-LSD, 5-HT-KET, and LSD-KET, each for the last 100 ns, respectively.

Analysis of membrane deformations and the residual mismatch. The properties of the membranes were analyzed from the simulation trajectories using the recently described CTMD method [32]. Briefly, to quantify membrane deformations in the simulations and the hydrophobic mismatch energies, we calculated the time-averaged hydrophobic thickness profile of the membrane surrounding 5-HT_{2A}R in all trajectories and used solvent accessible surface area calculations to calculate the energy of the residual mismatch which exposes TM residues participating in unfavorable interfacial hydrophobic/hydrophilic interactions.

References

- Gonzalez-Maeso J (2010) Anxious interactions. *Nat Neurosci* 13: 524–526.
- Nichols CD (2009) Serotonin 5-HT_{2A} Receptor Function as a Contributing Factor to Both Neuropsychiatric and Cardiovascular Diseases. *Cardiovasc Psychiatry Neurol* 2009: 475108.
- Gresch PJ, Strickland LV, Sanders-Bush E (2002) Lysergic acid diethylamide-induced Fos expression in rat brain: role of serotonin-2A receptors. *Neuroscience* 114: 707–713.
- Gonzalez-Maeso J, Yuen T, Ebersole BJ, Wurmbach E, Lira A, et al. (2003) Transcriptome fingerprints distinguish hallucinogenic and nonhallucinogenic 5-hydroxytryptamine 2A receptor agonist effects in mouse somatosensory cortex. *J Neurosci* 23: 8836–8843.
- Weinstein H (2005) Hallucinogen actions on 5-HT receptors reveal distinct mechanisms of activation and signaling by G protein-coupled receptors. *AAPS J* 7: E871–E884.
- Almaula N, Ebersole BJ, Zhang D, Weinstein H, Sealfon SC (1996) Mapping the binding site pocket of the serotonin 5-Hydroxytryptamine2A receptor. *Ser* 3.36(159) provides a second interaction site for the protonated amine of serotonin but not of lysergic acid diethylamide or bufofemine. *J Biol Chem* 271: 14672–14675.
- Ebersole BJ, Visiers I, Weinstein H, Sealfon SC (2003) Molecular basis of partial agonism: orientation of indoleamine ligands in the binding pocket of the human serotonin 5-HT2A receptor determines relative efficacy. *Mol Pharmacol* 63: 36–43.
- Chang C-w, Poteet E, Schetz JA, Gümüs ZH, Weinstein H (2009) Towards a quantitative representation of the cell signaling mechanisms of hallucinogens: Measurement and mathematical modeling of 5-HT1A and 5-HT2A receptor-mediated ERK1/2 activation. *Neuropharmacology* 56: 213–225.
- Kahsai AW, Xiao K, Rajagopal S, Ahn S, Shukla AK, et al. (2011) Multiple ligand-specific conformations of the β_2 -adrenergic receptor. *Nat Chem Biol* 7: 692–700.
- Visiers I, Ebersole BJ, Dracheva S, Ballesteros J, Sealfon SC, et al. (2002) Structural motifs as functional microdomains in G-protein-coupled receptors: Energetic considerations in the mechanism of activation of the serotonin 5-HT2A receptor by disruption of the ionic lock of the arginine cage. *Int J Quantum Chem* 88: 65–75.
- Li J, Huang P, Chen C, de Riel JK, Weinstein H, et al. (2001) Constitutive Activation of the μ Opioid Receptor by Mutation of D3.49(164), but Not D3.32(147): D3.49(164) Is Critical for Stabilization of the Inactive Form of the Receptor and for Its Expression. *Biochemistry* 40: 12039–12050.
- Kobilka BK (2007) G protein coupled receptor structure and activation. *Biochim Biophys Acta* 1768: 794–807.
- Deupi X, Kobilka B (2007) Activation of G Protein-Coupled Receptors. *Adv Protein Chem* 74: 137–166.
- Gether U (2000) Uncovering molecular mechanisms involved in activation of G protein-coupled receptors. *Endocr Rev* 21: 90–113.
- Visiers I, Ballesteros JA, Weinstein H (2002) Three-dimensional representations of G protein-coupled receptor structures and mechanisms. *Methods Enzymol* 343: 329–371.
- Park PS, Lodowski DT, Palczewski K (2008) Activation of G protein-coupled receptors: beyond two-state models and tertiary conformational changes. *Annu Rev Pharmacol Toxicol* 48: 107–141.
- Weis WI, Kobilka BK (2008) Structural insights into G-protein-coupled receptor activation. *Curr Opin Struct Biol* 18: 734–740.
- Ballesteros JA, Weinstein H (1995) Integrated Methods for Modeling G-Protein Coupled Receptors. *Methods Neurosci* 25: 366–428.
- Feierer J, Wirth M, Welte B, Schuessler S, Jochum M, et al. (2011) Helix 8 plays a crucial role in bradykinin B2 receptor trafficking and signaling. *J Biol Chem* 286: 43282–43293.
- Park JH, Scheerer P, Hofmann KP, Choe HW, Ernst OP (2008) Crystal structure of the ligand-free G-protein-coupled receptor opsin. *Nature* 454: 183–187.
- Scheerer P, Park JH, Hildebrand PW, Kim YJ, Krauss N, et al. (2008) Crystal structure of opsin in its G-protein-interacting conformation. *Nature* 455: 497–502.
- Han DS, Wang SX, Weinstein H (2008) Active state-like conformational elements in the beta2-AR and a photoactivated intermediate of rhodopsin identified by dynamic properties of GPCRs. *Biochemistry* 47: 7317–7321.
- Rasmussen SGF, Choi H-J, Fung JJ, Pardon E, Casarosa P, et al. (2011) Structure of a nanobody-stabilized active state of the β_2 adrenoceptor. *Nature* 469: 175–180.
- Prioleau C, Visiers I, Ebersole BJ, Weinstein H, Sealfon SC (2002) Conserved Helix 7 Tyrosine Acts as a Multistate Conformational Switch in the 5HT2C Receptor. Identification of a Novel “Locked-On” Phenotype and Double Revertant Mutations. *J Biol Chem* 277: 36577–36584.
- Rasmussen SGF, DeVree BT, Zou Y, Kruse AC, Chung KY, et al. (2011) Crystal structure of the β_2 adrenergic receptor-Gs protein complex. *Nature* 477: 549–555.
- Khelashvili G, Dorff K, Shan J, Camacho-Artacho M, Skrabaneck L, et al. (2010) GPCR-OKB: The G Protein Coupled Receptor Oligomer Knowledge Base. *Bioinformatics* 26: 2.
- Guo W, Shi L, Filizola M, Weinstein H, Javitch JA (2005) Crosstalk in G protein-coupled receptors: changes at the transmembrane homodimer interface determine activation. *Proc Natl Acad Sci U S A* 102: 17495–17500.
- Mancia F, Assur Z, Herman AG, Siegel R, Hendrickson WA (2008) Ligand sensitivity in dimeric associations of the serotonin 5HT2c receptor. *EMBO Rep* 9: 363–369.

To identify these residues, we determined if the TM is thicker or thinner than the surrounding membrane by comparing the hydrophobic thicknesses of the TM domains (using the following TM definitions (given in the Ballesteros-Weinstein generic numbering [18]): 1.29–1.59 (TM1), 2.38–2.67 (TM2), 3.24–3.53 (TM3), 4.39–4.63 (TM4), 5.38–5.63 (TM5), 6.33–6.59 (TM6), 7.30–7.56 (TM7)) to the local membrane thickness d_{memb} calculated from the membrane sectors corresponding to each TM, as described in [32].

Supporting Information

Text S1 Including supplemental methods, Figures S1, S2, S3, S4, S5, S6, Tables S1, S2, S3, Topology and parameter files for 5HT, LSD and KET.

(DOC)

Acknowledgments

We thank Dr. Junmei Wang for his assistance with the use of Antechamber.

Author Contributions

Conceived and designed the experiments: JS GK SM HW. Performed the experiments: JS SM. Analyzed the data: JS GK SM ELM HW. Contributed reagents/materials/analysis tools: SM ELM. Wrote the paper: JS GK SM ELM HW.

29. Moreno JL, Holloway T, Albizu L, Sealfon SC, Gonzalez-Maeso J (2011) Metabotropic glutamate mGlu2 receptor is necessary for the pharmacological and behavioral effects induced by hallucinogenic 5-HT2A receptor agonists. *Neurosci Lett* 493: 76–79.
30. Gonzalez-Maeso J, Ang RL, Yuen T, Chan P, Weisstaub NV, et al. (2008) Identification of a serotonin/glutamate receptor complex implicated in psychosis. *Nature* 452: 93–97.
31. Fung JJ, Deupi X, Pardo L, Yao XJ, Velez-Ruiz GA, et al. (2009) Ligand-regulated oligomerization of β_2 -adrenoceptors in a model lipid bilayer. *EMBO J* 28: 3315–3328.
32. Mondal S, Khelashvili G, Shan J, Andersen O, Weinstein H (2011) Quantitative modeling of membrane deformations by multi-helical membrane proteins: Application to G-protein Coupled Receptors. *Biophys J* 101: 2092–2101.
33. Schwartz TW, Frimurer TM, Holst B, Rosenkilde MM, Elling CE (2006) Molecular mechanism of 7TM receptor activation—a global toggle switch model. *Annu Rev Pharmacol Toxicol* 46: 481–519.
34. Farrens DL, Altenbach C, Yang K, Hubbell WL, Khorana HG (1996) Requirement of rigid-body motion of transmembrane helices for light activation of rhodopsin. *Science* 274: 768–770.
35. Ballesteros J, Kitano S, Guarneri F, Davies P, Fromme BJ, et al. (1998) Functional microdomains in G-protein-coupled receptors. The conserved arginine-cage motif in the gonadotropin-releasing hormone receptor. *J Biol Chem* 273: 10445–10453.
36. Ghannouni P, Steenhuys JJ, Farrens DL, Kobilka BK (2001) Agonist-induced conformational changes in the G-protein-coupling domain of the β_2 adrenergic receptor. *Proc Natl Acad Sci U S A* 98: 5997–6002.
37. Altenbach C, Kusnetzow AK, Ernst OP, Hofmann KP, Hubbell WL (2008) High-resolution distance mapping in rhodopsin reveals the pattern of helix movement due to activation. *Proc Natl Acad Sci U S A* 105: 7439–7444.
38. Lin SW, Sakmar TP (1996) Specific tryptophan UV-absorbance changes are probes of the transition of rhodopsin to its active state. *Biochemistry* 35: 11149–11159.
39. Sansom MS, Weinstein H (2000) Hinges, swivels and switches: the role of prolines in signalling via transmembrane alpha-helices. *Trends Pharmacol Sci* 21: 445–451.
40. Dror RO, Arlow DH, Borhani DW, Jensen MÅ, Piana S, et al. (2009) Identification of two distinct inactive conformations of the β_2 -adrenergic receptor reconciles structural and biochemical observations. *Proc Natl Acad Sci U S A* 106: 4689–4694.
41. Teller DC, Okada T, Behnke CA, Palczewski K, Stenkamp RE (2001) Advances in determination of a high-resolution three-dimensional structure of rhodopsin, a model of G-protein-coupled receptors (GPCRs). *Biochemistry* 40: 7761–7772.
42. van Aalten DM, Amadei A, Linssen AB, Eijssink VG, Vriend G, et al. (1995) The essential dynamics of thermolysin: confirmation of the hinge-bending motion and comparison of simulations in vacuum and water. *Proteins* 22: 45–54.
43. Khelashvili G, Grossfield A, Feller SE, Pitman MC, Weinstein H (2009) Structural and dynamic effects of cholesterol at preferred sites of interaction with rhodopsin identified from microsecond length molecular dynamics simulations. *Proteins* 76: 403–417.
44. Lyman E, Higgs C, Kim B, Lupyan D, Shelley JC, et al. (2009) A role for a specific cholesterol interaction in stabilizing the Apo configuration of the human A(2A) adenosine receptor. *Structure* 17: 1660–1668.
45. Cherezov V, Rosenbaum DM, Hanson MA, Rasmussen SG, Thian FS, et al. (2007) High-resolution crystal structure of an engineered human β_2 -adrenergic G protein-coupled receptor. *Science* 318: 1258–1265.
46. Hanson MA, Cherezov V, Griffith MT, Roth CB, Jaakola VP, et al. (2008) A specific cholesterol binding site is established by the 2.8 Å structure of the human beta2-adrenergic receptor. *Structure* 16: 897–905.
47. Goforth RL, Chi AK, Greathouse DV, Providence LL, Koeppe RE, et al. (2003) Hydrophobic coupling of lipid bilayer energetics to channel function. *J Gen Physiol* 121: 477.
48. Periole X, Huber T, Marrink SJ, Sakmar TP (2007) G protein-coupled receptors self-assemble in dynamics simulations of model bilayers. *J Am Chem Soc* 129: 10126–10132.
49. Morse M, Tran E, Sun H, Levenson R, Fang Y (2011) Ligand-directed functional selectivity at the mu opioid receptor revealed by label-free integrative pharmacology on-target. *PLoS One* 6: e25643.
50. Urban JD, Clarke WP, von Zastrow M, Nichols DE, Kobilka B, et al. (2007) Functional selectivity and classical concepts of quantitative pharmacology. *J Pharmacol Exp Ther* 320: 1–13.
51. Luttrell LM, Kenakin TP (2011) Refining efficacy: allosterism and bias in G protein-coupled receptor signaling. *Methods Mol Biol* 756: 3–35.
52. Gonzalez-Maeso J, Sealfon SC (2009) Agonist-Trafficking and Hallucinogens. *Curr Med Chem* 16: 1017–1027.
53. Yao X, Parnot C, Deupi X, Ratnala VR, Swaminath G, et al. (2006) Coupling ligand structure to specific conformational switches in the β_2 -adrenoceptor. *Nat Chem Biol* 2: 417–422.
54. Richard BM (2007) GPCR functional selectivity has therapeutic impact. *Trends Pharmacol Sci* 28: 390–396.
55. Kenakin T (2008) Functional selectivity in GPCR modulator screening. *Comb Chem High Throughput Screen* 11: 337–343.
56. Valant C, Gregory KJ, Hall NE, Scammells PJ, Lew MJ, et al. (2008) A Novel Mechanism of G Protein-coupled Receptor Functional Selectivity. *J Biol Chem* 283: 29312–29321.
57. Seifer R, Dove S (2009) Functional Selectivity of GPCR Ligand Stereoisomers: New Pharmacological Opportunities. *Mol Pharmacol* 75: 13–18.
58. Ward RJ, Jenkins L, Milligan G (2009) Selectivity and functional consequences of interactions of family A G protein-coupled receptors with neurochondrin and periplakin. *J Neurochem* 109: 182–192.
59. Peters MF, Scott CW (2009) Evaluating Cellular Impedance Assays for Detection of GPCR Pleiotropic Signaling and Functional Selectivity. *J Biomol Screen* 14: 246–255.
60. Leduc M, Breton B, Gales C, Le Gouill C, Bouvier M, et al. (2009) Functional Selectivity of Natural and Synthetic Prostaglandin EP4 Receptor Ligands. *J Pharmacol Exp Ther* 331: 297–307.
61. Stewart GD, Valant C, Dowell SJ, Mijajlic D, Devenish RJ, et al. (2009) Determination of Adenosine A1 Receptor Agonist and Antagonist Pharmacology Using *Saccharomyces cerevisiae*: Implications for Ligand Screening and Functional Selectivity. *J Pharmacol Exp Ther* 331: 277–286.
62. Bosier B, Muccioli GG, Hermans E, Lambert DM (2010) Functionally selective cannabinoid receptor signalling: Therapeutic implications and opportunities. *Bioche Pharmacol* 80: 1–12.
63. Stewart GD, Sexton PM, Christopoulos A (2010) Detection of Novel Functional Selectivity at M3 Muscarinic Acetylcholine Receptors Using a *Saccharomyces cerevisiae* Platform. *ACS Chem Biol* 5: 365–375.
64. Urizzi E, Yano H, Kolster R, Gales C, Lambert N, et al. (2011) CODA-RET reveals functional selectivity as a result of GPCR heteromerization. *Nat Chem Biol* 7: 624–630.
65. Provost D, Artacho MC, Negri A, Mobarec JC, Filizola M (2011) Ligand-Induced Modulation of the Free-Energy Landscape of G Protein-Coupled Receptors Explored by Adaptive Biasing Techniques. *PLoS Comput Biol* 7: e1002193.
66. Gesty-Palmer D, Luttrell LM (2011) Refining efficacy: exploiting functional selectivity for drug discovery. *Adv Pharmacol* 62: 79–107.
67. Abbas A, Roth BL (2008) Arresting serotonin. *Proc Natl Acad Sci U S A* 105: 831–832.
68. Kenakin T (2003) Ligand-selective receptor conformations revisited: the promise and the problem. *Trends Pharmacol Sci* 24: 346–354.
69. Farahbakhsh ZT, Hideg K, Hubbell WL (1993) Photoactivated conformational changes in rhodopsin: a time-resolved spin label study. *Science* 262: 1416–1419.
70. Nakanishi J, Takarada T, Yunoki S, Kikuchi Y, Maeda M (2006) FRET-based monitoring of conformational change of the beta2 adrenergic receptor in living cells. *Biochem Biophys Res Commun* 343: 1191–1196.
71. Weinstein H, Mazurek AP, Osman R, Topiol S (1986) Theoretical studies on the activation mechanism of the histamine H2-receptor: the proton transfer between histamine and a receptor model. *Mol Pharmacol* 29: 28–33.
72. Kovalainen JT, Christiansen JAM, Ropponen R, Poso A, Perakyla M, et al. (2000) A Proton Relay Process as the Mechanism of Activation of the Histamine H3-Receptor Determined by 1H NMR and ab Initio Quantum Mechanical Calculations. *J Am Chem Soc* 122: 6989–6996.
73. Salom D, Lodowski DT, Stenkamp RE, Le Trong I, Golczak M, et al. (2006) Crystal structure of a photoactivated deprotonated intermediate of rhodopsin. *Proc Natl Acad Sci U S A* 103: 16123–16128.
74. Fahmy K, Sakmar TP, Siebert F (2000) Transducin-dependent protonation of glutamic acid 134 in rhodopsin. *Biochemistry* 39: 10607–10612.
75. Niu SL, Mitchell DC, Litman BJ (2001) Optimization of receptor-G protein coupling by bilayer lipid composition II: formation of metarhodopsin II-transducin complex. *J Biol Chem* 276: 42807–42811.
76. Hurst DP, Grossfield A, Lynch DL, Feller S, Romo TD, et al. (2010) A lipid pathway for ligand binding is necessary for a cannabinoid G protein-coupled receptor. *J Biol Chem* 285: 17954–17964.
77. Romo TD, Grossfield A, Pitman MC (2010) Concerted interconversion between ionic lock substrates of the β_2 adrenergic receptor revealed by microsecond timescale molecular dynamics. *Biophys J* 98: 76–84.
78. Jastrzebska B, Debinski A, Filipk S, Palczewski K (2011) Role of membrane integrity on G protein-coupled receptors: Rhodopsin stability and function. *Prog Lipid Res* 50: 267–277.
79. Mertz B, Struts AV, Feller SE, Brown MF (2012) Molecular simulations and solid-state NMR investigate dynamical structure in rhodopsin activation. *Biochim Biophys Acta* 1818: 241–51.
80. Botelho AV, Huber T, Sakmar TP, Brown MF (2006) Curvature and hydrophobic forces drive oligomerization and modulate activity of rhodopsin in membranes. *Biophys J* 91: 4464–4477.
81. Moukhamedzhanov R, Warne T, Edwards PC, Serrano-Vega MJ, Leslie AGW, et al. (2011) Two distinct conformations of helix 6 observed in antagonist-bound structures of a β_1 -adrenergic receptor. *Proc Natl Acad Sci U S A* 108: 8228–8232.
82. Sali A, Blundell TL (1993) Comparative protein modelling by satisfaction of spatial restraints. *J Mol Biol* 234: 779–815.
83. Shan J, Weinstein H, Mehler EL (2010) Probing the Structural Determinants for the Function of Intracellular Loop 2 in Structurally Cognate G-Protein-Coupled Receptors. *Biochemistry* 49: 10691–10701.

84. Kortagere S, Roy A, Mehler EL (2006) Ab initio computational modeling of long loops in G-protein coupled receptors. *J Comput Aided Mol Des* 20: 427–436.
85. Mehler EL, Hassan SA, Kortagere S, Weinstein H (2006) *Ab initio* computational modeling of loops in G-protein-coupled receptors: lessons from the crystal structure of rhodopsin. *Proteins* 64: 673–690.
86. Goodsell DS, Morris GM, Olson AJ (1996) Automated Docking of Flexible Ligands: Applications of AutoDock. *J Mol Recognit* 9: 1.
87. Niv MY, Weinstein H (2005) A flexible docking procedure for the exploration of peptide binding selectivity to known structures and homology models of PDZ domains. *J Am Chem Soc* 127: 14072–14079.
88. Beuming T, Kniazeff J, Bergmann ML, Shi L, Gracia L, et al. (2008) The binding sites for cocaine and dopamine in the dopamine transporter overlap. *Nat Neurosci* 11: 780–789.
89. Friesner RA, Banks JL, Murphy RB, Halgren TA, Klicic JJ, et al. (2004) Glide: a new approach for rapid, accurate docking and scoring. 1. Method and assessment of docking accuracy. *J Med Chem* 47: 1739–1749.
90. Sherman W, Day T, Jacobson MP, Friesner RA, Farid R (2006) Novel procedure for modeling ligand/receptor induced fit effects. *J Med Chem* 49: 534–553.
91. Ho BY, Karschin A, Branchek T, Davidson N, Lester HA (1992) The role of conserved aspartate and serine residues in ligand binding and in function of the 5-HT_{1A} receptor: a site-directed mutation study. *FEBS Lett* 312: 259–262.
92. Roth BL, Shoham M, Choudhary MS, Khan N (1997) Identification of conserved aromatic residues essential for agonist binding and second messenger production at 5-hydroxytryptamine_{2A} receptors. *Mol Pharmacol* 52: 259–266.
93. Li J, Edwards PC, Burghammer M, Villa C, Schertler GF (2004) Structure of bovine rhodopsin in a trigonal crystal form. *J Mol Biol* 343: 1409–1438.
94. Murakami M, Kouyama T (2008) Crystal structure of squid rhodopsin. *Nature* 453: 363–367.
95. Jaakola VP, Griffith MT, Hanson MA, Cherezov V, Chien EY, et al. (2008) The 2.6 Å crystal structure of a human A_{2A} adenosine receptor bound to an antagonist. *Science* 322: 1211–1217.
96. Rosenbaum DM, Rasmussen SG, Kobilka BK (2009) The structure and function of G-protein-coupled receptors. *Nature* 459: 356–363.
97. Kentsis A, Mezei M, Osman R (2003) MC-PHS: a Monte Carlo implementation of the primary hydration shell for protein folding and design. *Biophys J* 84: 805–815.
98. Bennett MP, Mitchell DC (2008) Regulation of membrane proteins by dietary lipids: effects of cholesterol and docosahexaenoic acid acyl chain-containing phospholipids on rhodopsin stability and function. *Biophys J* 95: 1206–1216.
99. Humphrey W, Dalke A, Schulten K (1996) VMD: visual molecular dynamics. *J Mol Graph* 14: 33–38.
100. Mackerell AD, Jr., Feig M, Brooks CL, 3rd (2004) Extending the treatment of backbone energetics in protein force fields: limitations of gas-phase quantum mechanics in reproducing protein conformational distributions in molecular dynamics simulations. *J Comput Chem* 25: 1400–1415.
101. Brooks BR, Brooks CL, III, Mackerell AD, Jr., Nilsson L, Petrella RJ, et al. (2009) CHARMM: the biomolecular simulation program. *J Comput Chem* 30: 1545–1614.
102. Bayly CIC P, Cornell WD, Kollman PA (1993) A well-behaved electrostatic potential based method using charge restraints for deriving atomic charges: the RESP model. *J Phys Chem* 97: 10269–10280.
103. Wang J, Wang W, Kollman PA, Case DA (2006) Automatic atom type and bond type perception in molecular mechanical calculations. *J Mol Graph Model* 25: 247–260.
104. Guillet C, James TL (2008) Docking to RNA via root-mean-square-deviation-driven energy minimization with flexible ligands and flexible targets. *J Chem Inf Model* 48: 1257–1268.
105. Ge X, Roux B (2010) Absolute binding free energy calculations of sparsomycin analogs to the bacterial ribosome. *J Phys Chem B* 114: 9525–9539.
106. Phillips JC, Braun R, Wang W, Gumbart J, Tajkhorshid E, et al. (2005) Scalable molecular dynamics with NAMD. *J Comput Chem* 26: 1781–1802.
107. Shan J, Javitch JA, Shi L, Weinstein H (2011) The substrate-driven transition to an inward-facing conformation in the functional mechanism of the dopamine transporter. *PLoS One* 6: e16350.
108. Essmann U, Perera L, Berkowitz ML, Darden T, Lee H, et al. (1995) A Smooth Particle Mesh Ewald Method. *J Chem Phys* 103: 8577–8593.
109. Shi L, Quick M, Zhao Y, Weinstein H, Javitch JA (2008) The mechanism of a neurotransmitter:sodium symporter–inward release of Na⁺ and substrate is triggered by substrate in a second binding site. *Mol Cell* 30: 667–677.
110. Case DA, Darden TA, Cheatham III TE, Simmerling CL, Wang J, et al. (2006) AMBER 9. University of California, San Francisco.
111. Visiers I, Braunschweig BB, Weinstein H (2000) Prokink: a protocol for numerical evaluation of helix distortions by proline. *Protein Eng* 13: 603–606.
112. Mezei M (2010) Simulaid: A simulation facilitator and analysis program. *J Comput Chem* 31: 11.
113. Crawley MJ (2007) The R book. Chichester, West Sussex, England: John Wiley & Sons, Inc. 882 p.
114. Filizola M, Wang SX, Weinstein H (2006) Dynamic models of G-protein coupled receptor dimers: indications of asymmetry in the rhodopsin dimer from molecular dynamics simulations in a POPC bilayer. *J Comput Aided Mol Des* 20: 405–416.
115. Lindahl E, Hess B, van der Spoel D (2001) GROMACS 3.0: a package for molecular simulation and trajectory analysis. *J Mol Model* 7: 306–317.
116. Wang CD, Gallaher TK, Shih JC (1993) Site-directed mutagenesis of the serotonin 5-hydroxytryptamine₂ receptor: identification of amino acids necessary for ligand binding and receptor activation. *Mol Pharmacol* 43: 931–940.
117. Kristiansen K, Kroese WK, Willins DL, Gelber EI, Savage JE, et al. (2000) A highly conserved aspartic acid (Asp-155) anchors the terminal amine moiety of tryptamines and is involved in membrane targeting of the 5-HT_{2A} serotonin receptor but does not participate in activation via a “salt-bridge disruption” mechanism. *J Pharmacol Exp Ther* 293: 735–746.
118. Braden MR, Nichols DE (2007) Assessment of the roles of serines 5.43(239) and 5.46(242) for binding and potency of agonist ligands at the human serotonin 5-HT_{2A} receptor. *Mol Pharmacol* 72: 1200–1209.
119. Almula N, Ebersole BJ, Ballesteros JA, Weinstein H, Sealoff SC (1996) Contribution of a helix 5 locus to selectivity of hallucinogenic and nonhallucinogenic ligands for the human 5-hydroxytryptamine_{2A} and 5-hydroxytryptamine_{2C} receptors: direct and indirect effects on ligand affinity mediated by the same locus. *Mol Pharmacol* 50: 34–42.

TEXT S1

Ligand-dependent conformations and dynamics of the serotonin 5-HT_{2A} receptor determine its activation and membrane-driven oligomerization properties

Jufang Shan, George Khelashvili, Sayan Mondal, Ernest L. Mehler, Harel Weinstein

Supplemental Methods

Ab initio loop structure prediction with the Monte Carlo-Scaled Collective Variables method (MC-SCV)

Two rounds of loop calculations were carried out. First, loops were modeled separately and subjected to a protocol consisting of four steps of MC-SCV calculations (for details see ref. [1,2,3,4]). Step-1 uses MC-Simulated Annealing to generate an ensemble of folded loops from a fully extended polypeptide chain followed by 3 steps using MC-SCV; Step-2 performs opening-closing of the loops at 310 K in the field of protein and continuum solvent to relax the fold; Step-3 selects low energy loop conformations from Step-2, replicates them, opens, heats and closes each ensemble of loops at 1210 K, which facilitates crossing energy barriers and finding the native ensembles; and Step-4 selects low energy loops from Step-3, replicates them, and opens-closes each ensemble at 310K. The ensembles in Step-4 are ranked based on an Helmholtz-like free energy

$$\Delta A = E_{\min} - RT \ln Q \quad (1)$$

Where

$$Q = \sum_{i=1}^M \exp\left[-\frac{E_i - E_{\min}}{RT}\right] \quad (2)$$

with M denoting the number of replicas used in the MC calculation, and E_{\min} and E_i representing the minimum energy of the given ensemble, and the energy of the i 'th conformation in the distribution, respectively. The ensemble with the lowest ΔA is assumed to be the best representative of the native ensemble.

Extracellular loop 1 (EL1) and intracellular loop 1 (IL1) were not included in the first round, because they share similar (short) lengths with EL1 and IL1 in rhodopsin [5] and β_2 AR [6]. In addition, these loops in rhodopsin and β_2 AR share common structures as well (RMSD < 1.1 Å). Taken together, EL1 and IL1 in the three GPCRs, 5-HT_{2A}R, rhodopsin and β_2 AR, should be structurally similar.

For EL2, with a conserved disulfide bridge between its Cys227 and C3.25 (Ballesteros-Weinstein numbering [7]) a special protocol was developed that allowed the loop sequence to be split into two shorter segments. The first segment (EL2a) ran from the loop's N-terminus to the disulfide bridged Cys227 while the second segment (EL2b) ran from Cys227 to the loop's C-terminus peptide. Segment EL2b was calculated first and then EL2a was predicted in the presence of EL2b.

In the second round of calculations, all the loops were assembled and refined one by one in the order of IL2, IL3, IL1, and EL2, EL3, EL1. For EL1 and IL1, previous built homology

models [1] were used (see below) as initial structures. For IL2, a previously built helical structure [1] was used. In this round, the loops were only subjected to Step-2 (open-close at 310K) in order to relax them in the field of protein, solvent and other loops. EL2a and EL2b were opened and closed simultaneously using a special algorithm designed for the EL2 [2]. All the loops produced ensembles with small energy and RMSD spreads, indicating that they belonged to the native ensembles [3].

The sequences of the predicted loops are given in Supplemental Table S2. Note, that since the original IL3 is much longer compared to the other loops, and therefore difficult to investigate with *ab initio* methods, we truncated IL3 but still kept residues critical for G-protein coupling, arrestin binding and downstream signaling in cognate GPCRs [8,9,10,11]. GPCRs with such truncated IL3 or chimeric GPCRs consisting of TM1-5 and TM6-7 (without IL3) segments taken from different GPCRs are known to maintain ligand-related functional elements [12,13,14,15,16,17].

We note that, except for short and conserved loop segments EL1, IL1 and EL2b, the predicted loops are different from those of β_2 AR, although the transmembrane helices (TMs) from the homology model are similar to those in β_2 AR (with a backbone RMSD of 0.6 Å based on the main chain superposition of the seven I.50 residues). EL2a in 5-HT₂AR is shorter than that in β_2 AR, nonetheless it has some helical contents although shorter than the two-turn helix in β_2 AR. Our previous comparative study of the structural properties of IL2 in wild type β_1 AR, β_2 AR and 5-HT₂AR GPCRs, as well as in the corresponding P5.37A mutants showed the existence of at least two major conformational families for IL2 in the cognate GPCRs. Furthermore, we found that it is most likely the helical conformation that binds to β -arrestin and

therefore is a part of the active form of these GPCRs [1]. Thus, in our simulations of 5-HT_{2A}R with 5HT and LSD the IL2 conformation was helical similar to that in β₁AR [18]. Since 5-HT_{2A}R has some basal activity in the presence of KET, a helical IL2 was also used in the KET simulation.

Preferred Cholesterol binding sites around 5-HT_{2A}R and rhodopsin

To determine preferred cholesterol (Chol) binding sites around 5-HT_{2A}R, for each simulation, we first identified the Chol molecules in contact with the receptor as those within 2.5 Å of the protein at any time-point during the entire 350 ns simulations. In addition, we also tracked those Chol that were within 10 Å radial shell around 5-HT_{2A}R during the simulations. Note that the latter group of Chol molecules are not necessarily in direct contact with the GPCR. The Chol molecules were then classified according to the percentage of time they spend in contact with the protein (within 2.5 Å of the GPCR), as well as the percentage of time they reside within 10 Å radial shell around 5-HT_{2A}R. At the same time, the information was gathered about the protein residues nearest to the Chol. From the location of these residues we identified the TM regions participating in interactions with Chol.

The information gathered from this analysis is consolidated in the Table S1. Note that in addition to the three 5-HT_{2A}R sets of simulations, we performed a 250 ns simulation of rhodopsin in the same SDPC/POPC/Chol membrane. This new simulation was conducted in order to compare Chol dynamics around different GPCRs, as well as in different lipid membrane (IBM simulations, see [19,20]), with the ultimate goal of constructing a generalizable model of Chol involvement in GPCR function. *The entries in Table S1 are colored and labeled according to our Chol ranking described above (see captions for details).*

Supplemental Figures

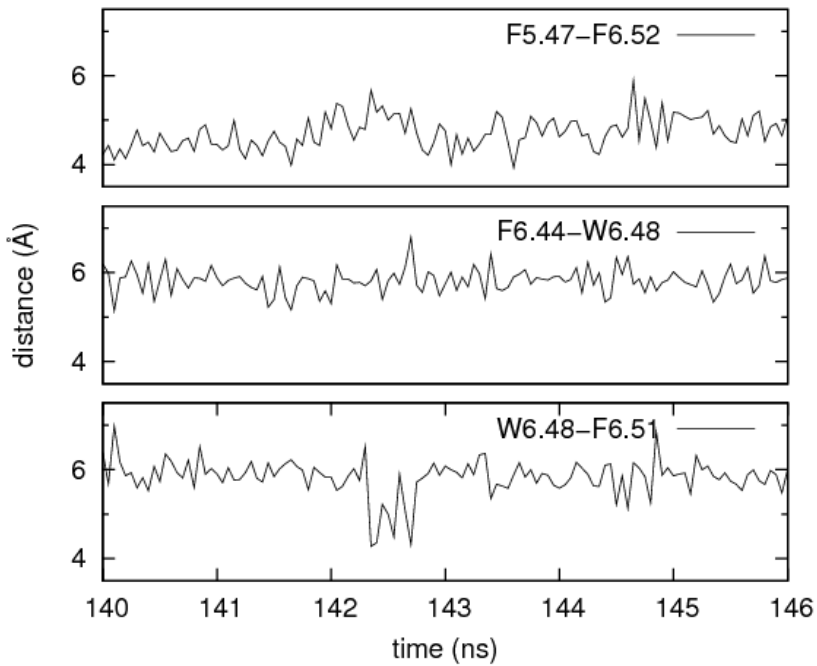


Figure S1. Distances between the centers of aromatic-residue rings in the 5-HT_{2A}R simulation. Some residues in the aromatic cluster form pi-pi interaction. Some of these interactions persist through the simulations (F5.47–F6.52) while others evolve with the flipping of W6.48, e.g., W6.48–F6.51.

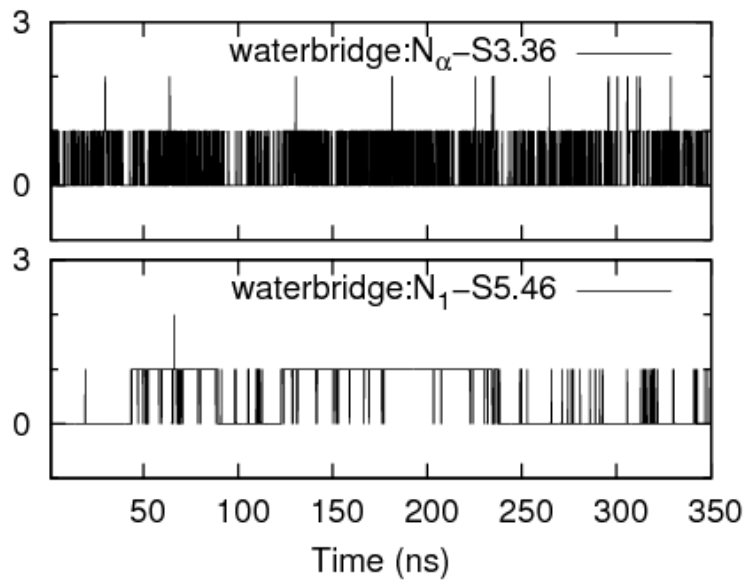


Figure S2. Number of water molecules between N_α on 5-HT and S3.36 of 5-HT_{2A}R (top panel), and between N₁ on 5-HT and S5.46 of 5-HT_{2A}R (bottom panel). Waters are counted if their oxygen are within 3.5 Å of both the nitrogen on 5-HT and hydroxyl oxygen of 5-HT_{2A}R. Data were collected every 100 ps.

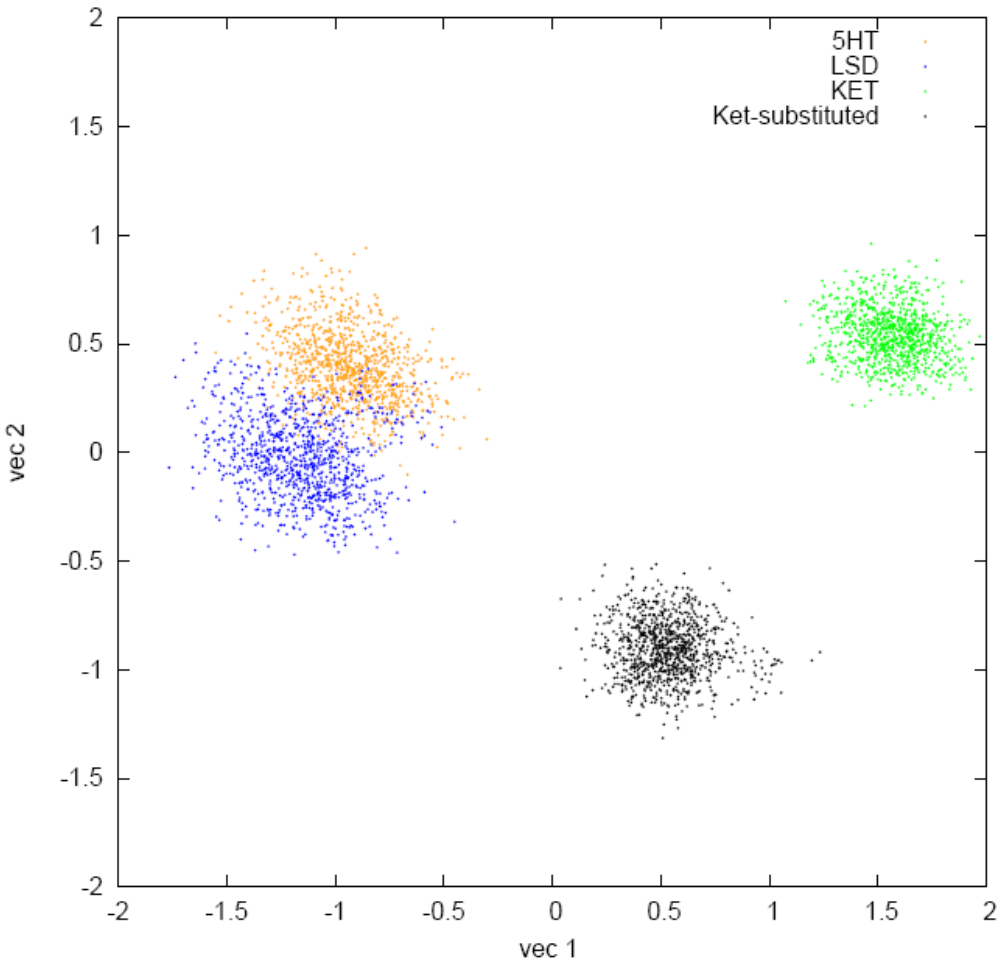


Figure S3. Comb-ED analysis performed on a concatenated trajectory composed of four separate simulations: 5-HT, LSD, KET and KET-substituted. The four simulations are in four distinct clusters and only the TM residues are followed. The largest variation among these four clusters is along the first eigenvector; 5HT and LSD are close to each other along this coordinate, but far away from Ket, while the Ket-substitution has already moved away from 5HT and LSD, and closer to KET. This is consistent with our observation, from monitoring RMSD and SM/FMs, that the substituted 5-HT-to-KET system is exhibiting dynamics similar to those produced by the inverse agonist.

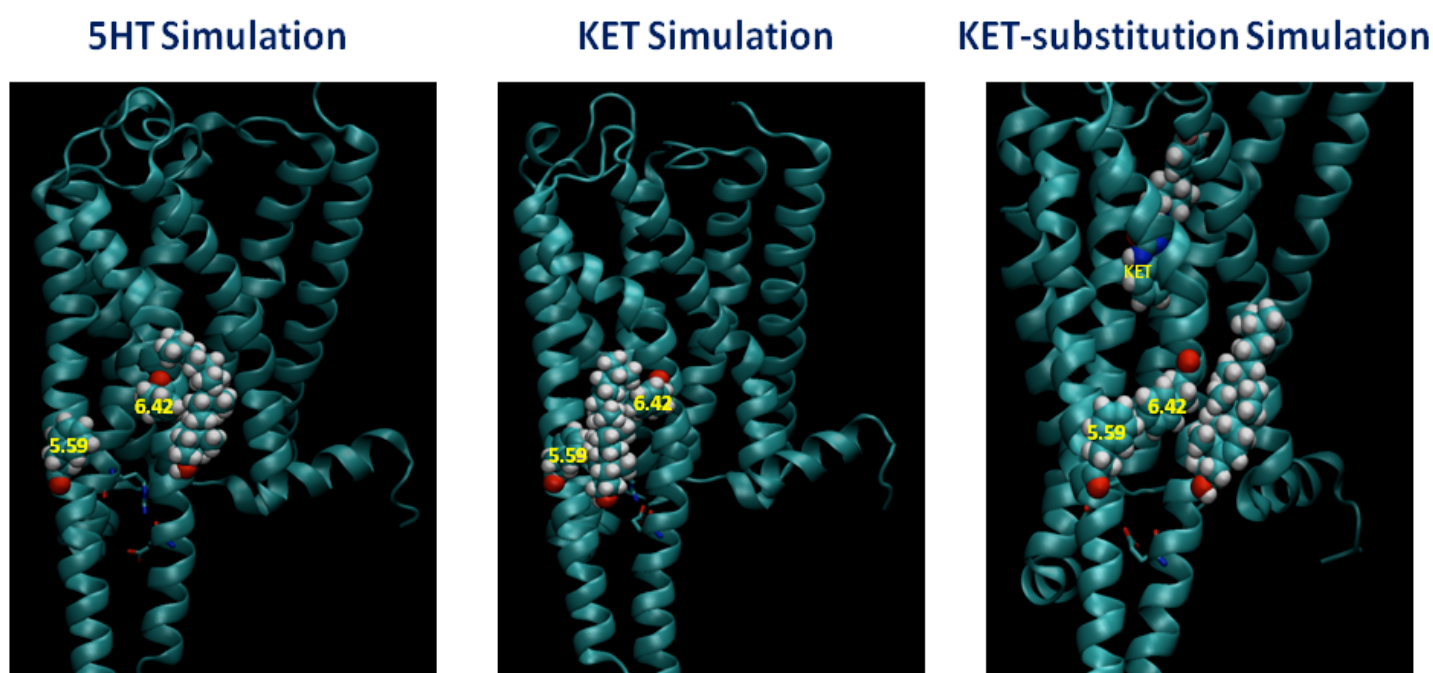


Figure S4. Snapshots of 5-HT_{2A}R conformations (shown in cartoon) stabilized by 5HT (left), KET (middle), and by KET substituted into 5HT structure (right). F5.59 and F6.42 residues on TM5 and TM6 respectively are in spheres. Cholesterol neighboring TM6 is in spheres. The ionic lock pair R3.50–E6.30 is depicted in licorice.

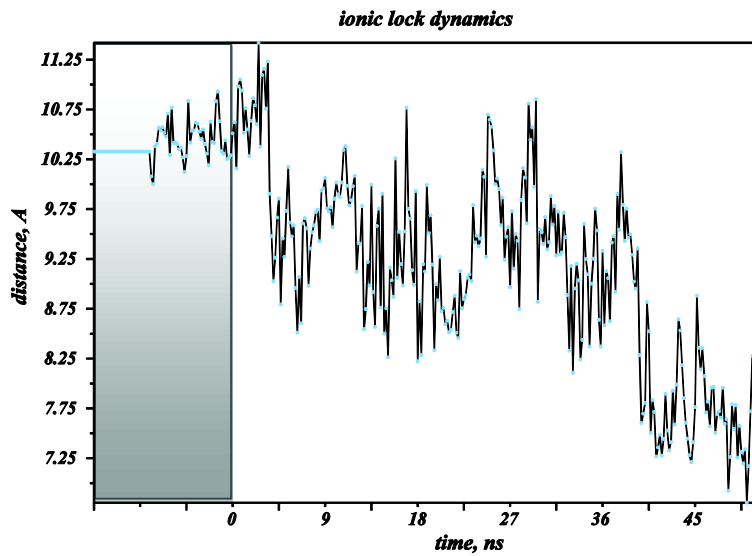


Figure S5. Distance between the C-alpha atoms of E6.30 and R3.50 residues in KET-bound 5HT_{2A}R simulations with protonated E6.30. The plot includes initial equilibration phase (shaded region), followed by ~55ns of unbiased simulations.

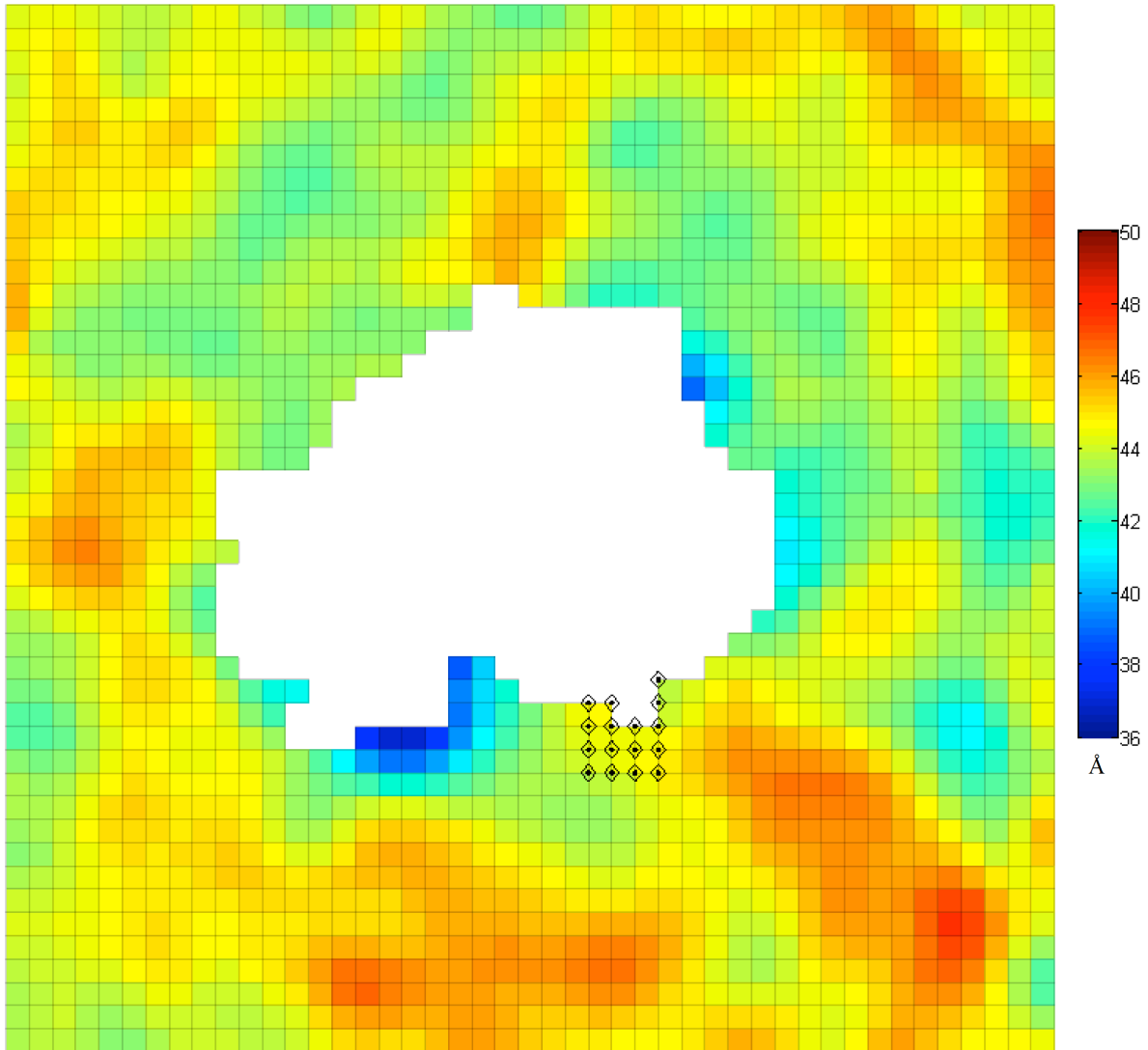


Figure S6. Hydrophobic thickness profile of the simulated membrane around 5-HT_{2AR} in complex with KET that substituted 5HT. Figure was prepared as Figure 8 and the membrane region near TM6 is highlighted.

Supplemental Tables

Table S1. Preferred Cholesterol binding sites around 5-HT_{2A}R and rhodopsin in mixed SDPC/POPC/Chol membranes

chol	5-HT _{2A} R						rhodopsin	
	5-HT		LSD		KET		11-cis-retinol	
	Inter. ^a	Region ^b	Inter. ^a	Region ^b	Inter. ^a	Region ^b	Inter. ^a	Region ^b
1	-				stays	EC/6		
2	transient		stays		stays	EC/6	stays	EC/5-6
3	stays		stays	EC/6	stays	EC/6	stays	EC/5-6
4	stays	EC/1	-		stays		stays	EC/5-6
5	stays		stays	EC/1	-		stays	-
6	stays	EC/1-2	stays	EC/1-2	stays	EC/1	stays	EC/5-6
7	stays		-		-		-	
8	out		-		transient		stays	EC/5-6
9	transient		-		stays	EC/1	transient	
10	stays	EC/2-3	stays	EC/2-3	stays	EC/2	stays	EC/1-2-3
11	stays	EC/3-4	stays	EC/3-4	stays	EC/4	stays	EC/1-2-3
12	stays	EC/2-3	-		-			
13	stays	EC/3	transient		transient	EC/4	out transient	
14	-		-		-			
15	stays		stays	EC/5	-		-	
16	stays		-		-		transient	EC/6-7
17	stays	IC/4	-		-		-	
18	stays		stays	IC/5	stays	IC/5-6	stays	IC5
19	out		-		-			IC/7-palm
20	stays	IC/6-7	stays	IC/6	-		stays	IC/6-7
21	stays	IC/7-8	stays	IC/1-7-8	stays	IC/1-7	stays	IC/6-7
22	out		stays	IC/1	stays			
23	stays	IC/3-5	stays		stays	IC/3-4-5	transient	
24	stays	IC/4	stays	IC/4	stays	IC/4	stays	IC124
25	stays		-		-		-	
26	stays	IC/1-2-4	stays	IC/2-4	stays	IC/1-2-4	stays	IC124
27	stays		-		-		stays transient	
28	transient		-		stays	IC/5	-	

^a Colors represent the extent of direct Chol-GPCR interactions: red, the Chol interacts (minimum distance < 2.5 Å) with the protein more than 75% of the time; green, between 25 and 75% of the time; grey, less than 25%. Labels (stays, in, out, transient) mean the percentage of time Chol

were found within 10 Å shell around the GPCR: “stays”, the Chol is in the shell more than 80% of the time; “in”, in the shell between 20% and 80% of the time, *entering the shell* at some point of the trajectory and *staying inside the shell* till the end; “out”, in the shell between 20% and 80% of the time, *leaving the shell* at certain time point and *staying outside the shell* till the end; “transient”, in the shell between 20% and 80% of the time; “-”, stays in the shell less than 20% of the time.

Table S2. Sequence for *ab initio* loop prediction

Loop	Sequence ^a
IL1	1.58 <u>SLEKKLQNAT</u> 2.39
EL1	2.66 <u>LYGYRWPLPSK</u> 3.23
IL2	3.54 <u>IQNPIHHSRFNSRT</u> 4.40
EL2	4.62 <u>FGLQDDSKVFKEGSCLLA</u> D5.35
IL3	5.68 <u>EATLCVSD</u> 5.75--AA-- 6.21 <u>RRTMQSISNE</u> 6.30
EL3	6.61 <u>CKESCNEDVIG</u> 7.32

^a underlined are helical residues at the ends of corresponding TMs; italicized are residues only included in the second round of MC calculation; “--” designates truncations.

Table S3. Residual Exposures (SA_{res}) in the KET-substituted system

TM	SA _{res} (Å ²)
1	95
2	0
3	N.D.*
4	96
5	85
6	0
7	3.6

* N.D., Not Determined

Topology and parameter files for 5HT, LSD and KET

Topology file for 5HT

RESIDUE 5HT 1.0 ! serotonin, protonated.

GROUP

ATOM C1 CT2 -0.217
 ATOM H11 HA 0.267 !
 ATOM H12 HA 0.272 ! ! H1 | H11 H21 | C5 | H61
 GROUP ATOM C2 CT2 -0.483 ! | | | / \ /
 ATOM H21 HA 0.252 ! H2---N1---C1---C2---C3---C4 C6---O1
 ATOM H22 HA 0.253 ! | | | | | |
 GROUP ATOM C3 CY -0.181 ! H3 / \ / \ /
 ATOM C4 CPT -0.079 ! H01 N2 C8
 ATOM C9 CPT 0.154 ! | |
 ATOM N2 NY -0.623 ! H91 H81
 ATOM H91 H 0.456
 ATOM C10 CA 0.052
 ATOM H01 HP 0.247
 GROUP ATOM C5 CA -0.296
 ATOM H51 HP 0.241
 GROUP ATOM C6 CA 0.356
 ATOM O1 OH1 -0.765
 ATOM H61 H 0.508
 GROUP ATOM C7 CA -0.307
 ATOM H71 HP 0.252
 GROUP ATOM C8 CA -0.221
 ATOM H81 HP 0.257
 GROUP ATOM N1 NH3 -0.840
 ATOM H1 HC 0.482
 ATOM H2 HC 0.483
 ATOM H3 HC 0.480
 BOND C1 H11 C1 H12 C1 N1 N1 H1
 BOND C1 C2 N1 H2 N1 H3
 BOND C2 H21 C2 H22 C3 C4 C10 H01
 BOND C2 C3 C3 C10 C4 C5 C4 C9
 BOND C5 H51 C5 C6 C6 C7 C6 O1
 BOND O1 H61 C7 C8 C7 H71 C8 C9
 BOND C8 H81 C9 N2 N2 H91 N2 C10
 DONO H1 N1
 DONO H2 N1
 DONO H3 N1
 DONO H91 N2
 DONO H61 O1
 ACCE O1

! Internal coordinate definitions

IC	H1	N1	C1	C2	0.0000	0.00	60.00	0.00	0.0000
IC	N1	C1	C2	C3	0.0000	0.00	187.00	0.00	0.0000
IC	C1	C2	C3	C10	0.0000	0.00	253.50	0.00	0.0000
IC	H61	O1	C6	C5	0.0000	0.00	180.00	0.00	0.0000
IC	C4	C10	*C3	C2	0.0000	0.00	180.00	0.00	0.0000
IC	C9	C4	C3	C10	0.0000	0.00	0.00	0.00	0.0000
IC	C3	C4	C9	N2	0.0000	0.00	0.00	0.00	0.0000
IC	C9	C3	*C4	C5	0.0000	0.00	180.00	0.00	0.0000
IC	C9	C4	C5	C6	0.0000	0.00	0.00	0.00	0.0000
IC	C4	C5	C6	C7	0.0000	0.00	0.00	0.00	0.0000
IC	C5	C6	C7	C8	0.0000	0.00	0.00	0.00	0.0000
IC	C4	C6	*C5	H51	0.0000	0.00	180.00	0.00	0.0000
IC	C7	C5	*C6	O1	0.0000	0.00	180.00	0.00	0.0000
IC	C6	C8	*C7	H71	0.0000	0.00	180.00	0.00	0.0000
IC	C9	C7	*C8	H81	0.0000	0.00	180.00	0.00	0.0000
IC	C10	C9	*N2	H91	0.0000	0.00	180.00	0.00	0.0000
IC	N2	C3	*C10	H01	0.0000	0.00	180.00	0.00	0.0000
IC	C1	C3	*C2	H21	0.0000	0.00	240.00	0.00	0.0000
IC	C1	C3	*C2	H22	0.0000	0.00	120.00	0.00	0.0000
IC	N1	C2	*C1	H11	0.0000	0.00	118.00	0.00	0.0000
IC	N1	C2	*C1	H12	0.0000	0.00	-118.00	0.00	0.0000
IC	H1	C1	*N1	H2	0.0000	0.00	120.00	0.00	0.0000
IC	H1	C1	*N1	H3	0.0000	0.00	240.00	0.00	0.0000
IC	C7	C8	C9	C4	0.0000	0.00	0.00	0.00	0.0000
IC	H81	C8	C9	C4	0.0000	0.00	180.00	0.00	0.0000
IC	C7	C8	C9	N2	0.0000	0.00	180.00	0.00	0.0000
IC	C8	C9	C4	C5	0.0000	0.00	0.00	0.00	0.0000
IC	N2	C9	C4	C5	0.0000	0.00	180.00	0.00	0.0000
IC	C8	C9	C4	C3	0.0000	0.00	180.00	0.00	0.0000
IC	C4	C3	C10	N2	0.0000	0.00	0.00	0.00	0.0000
IC	C3	C10	N2	C9	0.0000	0.00	0.00	0.00	0.0000
IC	H01	C10	N2	C9	0.0000	0.00	180.00	0.00	0.0000
IC	C3	C10	N2	H91	0.0000	0.00	180.00	0.00	0.0000
IC	C10	N2	C9	C8	0.0000	0.00	180.00	0.00	0.0000
IC	H91	N2	C9	C8	0.0000	0.00	0.00	0.00	0.0000
IC	C10	N2	C9	C4	0.0000	0.00	0.00	0.00	0.0000
IC	C3	C4	C5	C6	0.0000	0.00	180.00	0.00	0.0000
IC	C9	C4	C5	H51	0.0000	0.00	180.00	0.00	0.0000
IC	H51	C5	C6	C7	0.0000	0.00	180.00	0.00	0.0000
IC	C4	C5	C6	O1	0.0000	0.00	180.00	0.00	0.0000
IC	O1	C6	C7	C8	0.0000	0.00	180.00	0.00	0.0000
IC	O1	C6	C7	H71	0.0000	0.00	0.00	0.00	0.0000
IC	C5	C4	C3	C2	0.0000	0.00	0.00	0.00	0.0000
IC	C9	C4	C3	C2	0.0000	0.00	180.00	0.00	0.0000
IC	N2	C10	C3	C2	0.0000	0.00	180.00	0.00	0.0000
IC	H21	C2	C3	C10	0.0000	0.00	15.00	0.00	0.0000
IC	H22	C2	C3	C10	0.0000	0.00	133.00	0.00	0.0000

Parameter file for 5-HT

ANGLES

CT2 CT2 CY 51.800 107.5000 ! from CT1 CT2 CA (PAR27)

DIHEDRALS

CT2 CT2 CY CA 0.2300 2 180.00 ! from CT1 CT2 CY CA (PAR27)
 CT2 CT2 CY CPT 0.2300 2 180.00 ! from CT1 CT2 CY CPT (PAR27)

OH1 CA CA CPT 3.1000 2 180.00 ! from OH1 CA CA CA (PAR27)

Topology file for LSD

* Topology File.

*

99 1
MASS 1 lna 14.010000
MASS 2 lcc 12.010000
MASS 3 lcd 12.010000
MASS 4 lc3 12.010000
MASS 5 ln4 14.010000
MASS 6 lc2 12.010000
MASS 7 lce 12.010000
MASS 8 lca 12.010000
MASS 9 lc 12.010000
MASS 10 lo 16.000000
MASS 11 ln 14.010000
MASS 12 lhn 1.008000
MASS 13 lh4 1.008000
MASS 14 lhc 1.008000
MASS 15 lhx 1.008000
MASS 16 lha 1.008000
MASS 17 lh1 1.008000

RESI LSD 1.000

GROUP

ATOM N1 lna -0.441808
ATOM C1 lcc -0.146181
ATOM C2 lcd -0.062140
ATOM C3 lc3 -0.088815
ATOM C4 lc3 -0.043140
ATOM N2 ln4 0.054172
ATOM C5 lc3 -0.637333
ATOM C6 lc3 0.037135
ATOM C7 lc2 -0.309572
ATOM C8 lce 0.105239
ATOM C9 lca -0.054047
ATOM C10 lca -0.212485
ATOM C11 lca -0.128160
ATOM C12 lca -0.263226
ATOM C13 lca 0.219139
ATOM C14 lca 0.056464
ATOM C15 lc3 -0.224743
ATOM H1 lhn 0.396704
ATOM H2 lh4 0.215196
ATOM H3 lhc 0.070140
ATOM H4 lhc 0.070140
ATOM H5 lhx 0.159003
ATOM H6 lhn 0.303609
ATOM H7 lhx 0.286079
ATOM H8 lhx 0.286079
ATOM H9 lhc 0.104687
ATOM H10 lha 0.170235
ATOM H11 lha 0.165798
ATOM H12 lha 0.162944

ATOM	H13	lha	0.187989	
ATOM	H14	lhx	0.141964	
ATOM	H15	lhx	0.141964	
ATOM	H16	lhx	0.141964	
GROUP				
ATOM	C16	lc	0.682278	
ATOM	O1	lo	-0.580329	
ATOM	N3	ln	-0.408838	
ATOM	C17	lc3	0.099247	
ATOM	C18	lc3	-0.172798	
ATOM	C19	lc3	0.099247	
ATOM	C20	lc3	-0.172798	
ATOM	H17	lh1	0.059829	
ATOM	H18	lh1	0.059829	
ATOM	H19	lhc	0.058280	
ATOM	H20	lhc	0.058280	
ATOM	H21	lhc	0.058280	
ATOM	H22	lh1	0.059829	
ATOM	H23	lh1	0.059829	
ATOM	H24	lhc	0.058280	
ATOM	H25	lhc	0.058280	
ATOM	H26	lhc	0.058280	
BOND	N1	C1	! dist	1.3753
BOND	N1	C13	! dist	1.3730
BOND	N1	H1	! dist	0.9936
BOND	C1	C2	! dist	1.3513
BOND	C1	H2	! dist	1.0710
BOND	C2	C3	! dist	1.4983
BOND	C2	C14	! dist	1.4210
BOND	C3	C4	! dist	1.5521
BOND	C3	H3	! dist	1.0897
BOND	C3	H4	! dist	1.0830
BOND	C4	N2	! dist	1.5175
BOND	C4	C8	! dist	1.5333
BOND	C4	H5	! dist	1.0833
BOND	N2	C5	! dist	1.5020
BOND	N2	C15	! dist	1.4939
BOND	N2	H6	! dist	1.0088
BOND	C5	C6	! dist	1.5188
BOND	C5	H7	! dist	1.0796
BOND	C5	H8	! dist	1.0769
BOND	C6	C7	! dist	1.5100
BOND	C6	C16	! dist	1.5411
BOND	C6	H9	! dist	1.0863
BOND	C7	C8	! dist	1.3242
BOND	C7	H10	! dist	1.0739
BOND	C8	C9	! dist	1.4847
BOND	C9	C10	! dist	1.3792
BOND	C9	C14	! dist	1.3896
BOND	C10	C11	! dist	1.4061
BOND	C10	H11	! dist	1.0752
BOND	C11	C12	! dist	1.3806
BOND	C11	H12	! dist	1.0745
BOND	C12	C13	! dist	1.3934
BOND	C12	H13	! dist	1.0749

BOND	C13	C14	! dist	1.3875
BOND	C15	H14	! dist	1.0760
BOND	C15	H15	! dist	1.0800
BOND	C15	H16	! dist	1.0789
BOND	C16	O1	! dist	1.2052
BOND	C16	N3	! dist	1.3418
BOND	N3	C17	! dist	1.4613
BOND	N3	C19	! dist	1.4701
BOND	C17	C18	! dist	1.5269
BOND	C17	H17	! dist	1.0822
BOND	C17	H18	! dist	1.0808
BOND	C18	H19	! dist	1.0854
BOND	C18	H20	! dist	1.0858
BOND	C18	H21	! dist	1.0833
BOND	C19	C20	! dist	1.5240
BOND	C19	H22	! dist	1.0817
BOND	C19	H23	! dist	1.0782
BOND	C20	H24	! dist	1.0850
BOND	C20	H25	! dist	1.0828
BOND	C20	H26	! dist	1.0855
ANGL	N1	C1	C2	! angle 109.4432
ANGL	N1	C1	H2	! angle 120.0153
ANGL	N1	C13	C12	! angle 133.9955
ANGL	N1	C13	C14	! angle 106.0941
ANGL	C1	N1	C13	! angle 109.4986
ANGL	C1	N1	H1	! angle 124.5972
ANGL	C1	C2	C3	! angle 135.1931
ANGL	C1	C2	C14	! angle 106.1710
ANGL	C2	C1	H2	! angle 130.5403
ANGL	C2	C3	C4	! angle 108.5341
ANGL	C2	C3	H3	! angle 110.6293
ANGL	C2	C3	H4	! angle 111.0958
ANGL	C2	C14	C9	! angle 128.0029
ANGL	C2	C14	C13	! angle 108.7911
ANGL	C3	C2	C14	! angle 118.6293
ANGL	C3	C4	N2	! angle 109.0449
ANGL	C3	C4	C8	! angle 113.6130
ANGL	C3	C4	H5	! angle 109.1609
ANGL	C4	C3	H3	! angle 108.5930
ANGL	C4	C3	H4	! angle 110.3968
ANGL	C4	N2	C5	! angle 112.6363
ANGL	C4	N2	C15	! angle 112.8902
ANGL	C4	N2	H6	! angle 106.7054
ANGL	C4	C8	C7	! angle 123.0242
ANGL	C4	C8	C9	! angle 113.5819
ANGL	N2	C4	C8	! angle 110.5523
ANGL	N2	C4	H5	! angle 105.3800
ANGL	N2	C5	C6	! angle 110.0178
ANGL	N2	C5	H7	! angle 107.4750
ANGL	N2	C5	H8	! angle 107.6363
ANGL	N2	C15	H14	! angle 110.2668
ANGL	N2	C15	H15	! angle 108.3661
ANGL	N2	C15	H16	! angle 108.5954
ANGL	C5	N2	C15	! angle 109.5614
ANGL	C5	N2	H6	! angle 107.4882

ANGL	C5	C6	C7	! angle	109.3831
ANGL	C5	C6	C16	! angle	107.3402
ANGL	C5	C6	H9	! angle	109.4278
ANGL	C6	C5	H7	! angle	111.8197
ANGL	C6	C5	H8	! angle	110.7998
ANGL	C6	C7	C8	! angle	124.2526
ANGL	C6	C7	H10	! angle	117.0804
ANGL	C6	C16	O1	! angle	117.7455
ANGL	C6	C16	N3	! angle	118.8528
ANGL	C7	C6	C16	! angle	110.4020
ANGL	C7	C6	H9	! angle	110.3583
ANGL	C7	C8	C9	! angle	123.3911
ANGL	C8	C4	H5	! angle	108.7552
ANGL	C8	C7	H10	! angle	118.6367
ANGL	C8	C9	C10	! angle	127.4960
ANGL	C8	C9	C14	! angle	115.4560
ANGL	C9	C10	C11	! angle	119.9982
ANGL	C9	C10	H11	! angle	121.2385
ANGL	C9	C14	C13	! angle	123.1983
ANGL	C10	C9	C14	! angle	117.0255
ANGL	C10	C11	C12	! angle	122.7864
ANGL	C10	C11	H12	! angle	118.4169
ANGL	C11	C10	H11	! angle	118.7463
ANGL	C11	C12	C13	! angle	117.0730
ANGL	C11	C12	H13	! angle	120.7039
ANGL	C12	C11	H12	! angle	118.7901
ANGL	C12	C13	C14	! angle	119.9093
ANGL	C13	N1	H1	! angle	125.9013
ANGL	C13	C12	H13	! angle	122.2203
ANGL	C15	N2	H6	! angle	107.2322
ANGL	C16	C6	H9	! angle	109.8717
ANGL	C16	N3	C17	! angle	125.7047
ANGL	C16	N3	C19	! angle	117.4011
ANGL	O1	C16	N3	! angle	123.3971
ANGL	N3	C17	C18	! angle	113.3349
ANGL	N3	C17	H17	! angle	107.1056
ANGL	N3	C17	H18	! angle	110.2610
ANGL	N3	C19	C20	! angle	112.6052
ANGL	N3	C19	H22	! angle	107.1764
ANGL	N3	C19	H23	! angle	108.3888
ANGL	C17	N3	C19	! angle	116.8850
ANGL	C17	C18	H19	! angle	110.1494
ANGL	C17	C18	H20	! angle	111.4038
ANGL	C17	C18	H21	! angle	111.3140
ANGL	C18	C17	H17	! angle	109.8598
ANGL	C18	C17	H18	! angle	110.2334
ANGL	C19	C20	H24	! angle	109.9804
ANGL	C19	C20	H25	! angle	110.6404
ANGL	C19	C20	H26	! angle	111.4165
ANGL	C20	C19	H22	! angle	110.4435
ANGL	C20	C19	H23	! angle	110.3281
ANGL	H3	C3	H4	! angle	107.5647
ANGL	H7	C5	H8	! angle	108.9455
ANGL	H14	C15	H15	! angle	110.2648
ANGL	H14	C15	H16	! angle	109.4673
ANGL	H15	C15	H16	! angle	109.8519

ANGL	H17	C17	H18		! angle	105.7216
ANGL	H19	C18	H20		! angle	108.1356
ANGL	H19	C18	H21		! angle	107.9830
ANGL	H20	C18	H21		! angle	107.7214
ANGL	H22	C19	H23		! angle	107.7224
ANGL	H24	C20	H25		! angle	108.1470
ANGL	H24	C20	H26		! angle	107.8451
ANGL	H25	C20	H26		! angle	108.7082
DIHE	C13	N1	C1	C2	! dihe	-0.4715
DIHE	H1	N1	C1	C2	! dihe	-179.8779
DIHE	C13	N1	C1	H2	! dihe	179.8900
DIHE	H1	N1	C1	H2	! dihe	0.4836
DIHE	C1	N1	C13	C12	! dihe	-179.3066
DIHE	H1	N1	C13	C12	! dihe	0.0902
DIHE	C1	N1	C13	C14	! dihe	0.3048
DIHE	H1	N1	C13	C14	! dihe	179.7015
DIHE	N1	C1	C2	C3	! dihe	-178.5838
DIHE	H2	C1	C2	C3	! dihe	1.0043
DIHE	N1	C1	C2	C14	! dihe	0.4284
DIHE	H2	C1	C2	C14	! dihe	-179.9835
DIHE	C1	C2	C3	C4	! dihe	-153.8976
DIHE	C14	C2	C3	C4	! dihe	27.1833
DIHE	C1	C2	C3	H3	! dihe	87.0548
DIHE	C14	C2	C3	H3	! dihe	-91.8644
DIHE	C1	C2	C3	H4	! dihe	-32.3420
DIHE	C14	C2	C3	H4	! dihe	148.7389
DIHE	C1	C2	C14	C9	! dihe	178.7625
DIHE	C3	C2	C14	C9	! dihe	-2.0306
DIHE	C1	C2	C14	C13	! dihe	-0.2399
DIHE	C3	C2	C14	C13	! dihe	178.9671
DIHE	C2	C3	C4	N2	! dihe	-175.0091
DIHE	H3	C3	C4	N2	! dihe	-54.6886
DIHE	H4	C3	C4	N2	! dihe	63.0077
DIHE	C2	C3	C4	C8	! dihe	-51.2131
DIHE	H3	C3	C4	C8	! dihe	69.1075
DIHE	H4	C3	C4	C8	! dihe	-173.1963
DIHE	C2	C3	C4	H5	! dihe	70.3467
DIHE	H3	C3	C4	H5	! dihe	-169.3328
DIHE	H4	C3	C4	H5	! dihe	-51.6365
DIHE	C3	C4	N2	C5	! dihe	165.7671
DIHE	C8	C4	N2	C5	! dihe	40.1770
DIHE	H5	C4	N2	C5	! dihe	-77.1627
DIHE	C3	C4	N2	C15	! dihe	-69.4941
DIHE	C8	C4	N2	C15	! dihe	164.9157
DIHE	H5	C4	N2	C15	! dihe	47.5760
DIHE	C3	C4	N2	H6	! dihe	48.0513
DIHE	C8	C4	N2	H6	! dihe	-77.5389
DIHE	H5	C4	N2	H6	! dihe	165.1214
DIHE	C3	C4	C8	C7	! dihe	-129.1667
DIHE	N2	C4	C8	C7	! dihe	-6.1942
DIHE	H5	C4	C8	C7	! dihe	109.0476
DIHE	C3	C4	C8	C9	! dihe	51.4208
DIHE	N2	C4	C8	C9	! dihe	174.3934
DIHE	H5	C4	C8	C9	! dihe	-70.3648
DIHE	C4	N2	C5	C6	! dihe	-64.5349

DIHE	C15	N2	C5	C6	! dihe	168.9228
DIHE	H6	N2	C5	C6	! dihe	52.7181
DIHE	C4	N2	C5	H7	! dihe	173.4987
DIHE	C15	N2	C5	H7	! dihe	46.9565
DIHE	H6	N2	C5	H7	! dihe	-69.2482
DIHE	C4	N2	C5	H8	! dihe	56.2888
DIHE	C15	N2	C5	H8	! dihe	-70.2534
DIHE	H6	N2	C5	H8	! dihe	173.5419
DIHE	C4	N2	C15	H14	! dihe	57.8961
DIHE	C5	N2	C15	H14	! dihe	-175.7058
DIHE	H6	N2	C15	H14	! dihe	-59.3391
DIHE	C4	N2	C15	H15	! dihe	-62.8761
DIHE	C5	N2	C15	H15	! dihe	63.5220
DIHE	H6	N2	C15	H15	! dihe	179.8887
DIHE	C4	N2	C15	H16	! dihe	177.8343
DIHE	C5	N2	C15	H16	! dihe	-55.7676
DIHE	H6	N2	C15	H16	! dihe	60.5991
DIHE	N2	C5	C6	C7	! dihe	50.5236
DIHE	H7	C5	C6	C7	! dihe	169.8724
DIHE	H8	C5	C6	C7	! dihe	-68.3793
DIHE	N2	C5	C6	C16	! dihe	170.3251
DIHE	H7	C5	C6	C16	! dihe	-70.3260
DIHE	H8	C5	C6	C16	! dihe	51.4223
DIHE	N2	C5	C6	H9	! dihe	-70.4838
DIHE	H7	C5	C6	H9	! dihe	48.8650
DIHE	H8	C5	C6	H9	! dihe	170.6134
DIHE	C5	C6	C7	C8	! dihe	-17.8300
DIHE	C16	C6	C7	C8	! dihe	-135.7317
DIHE	H9	C6	C7	C8	! dihe	102.6107
DIHE	C5	C6	C7	H10	! dihe	160.1342
DIHE	C16	C6	C7	H10	! dihe	42.2325
DIHE	H9	C6	C7	H10	! dihe	-79.4250
DIHE	C5	C6	C16	O1	! dihe	-23.8245
DIHE	C7	C6	C16	O1	! dihe	95.3248
DIHE	H9	C6	C16	O1	! dihe	-142.7302
DIHE	C5	C6	C16	N3	! dihe	156.9304
DIHE	C7	C6	C16	N3	! dihe	-83.9203
DIHE	H9	C6	C16	N3	! dihe	38.0247
DIHE	C6	C7	C8	C4	! dihe	-4.7193
DIHE	H10	C7	C8	C4	! dihe	177.3459
DIHE	C6	C7	C8	C9	! dihe	174.6357
DIHE	H10	C7	C8	C9	! dihe	-3.2990
DIHE	C4	C8	C9	C10	! dihe	153.9871
DIHE	C7	C8	C9	C10	! dihe	-25.4229
DIHE	C4	C8	C9	C14	! dihe	-24.2233
DIHE	C7	C8	C9	C14	! dihe	156.3667
DIHE	C8	C9	C10	C11	! dihe	-179.1234
DIHE	C14	C9	C10	C11	! dihe	-0.9373
DIHE	C8	C9	C10	H11	! dihe	-0.6468
DIHE	C14	C9	C10	H11	! dihe	177.5393
DIHE	C8	C9	C14	C2	! dihe	-0.2611
DIHE	C10	C9	C14	C2	! dihe	-178.6673
DIHE	C8	C9	C14	C13	! dihe	178.6102
DIHE	C10	C9	C14	C13	! dihe	0.2040
DIHE	C9	C10	C11	C12	! dihe	0.9516
DIHE	H11	C10	C11	C12	! dihe	-177.5628

DIHE	C9	C10	C11	H12	! dihe	-179.9927
DIHE	H11	C10	C11	H12	! dihe	1.4929
DIHE	C10	C11	C12	C13	! dihe	-0.1604
DIHE	H12	C11	C12	C13	! dihe	-179.2127
DIHE	C10	C11	C12	H13	! dihe	179.2527
DIHE	H12	C11	C12	H13	! dihe	0.2004
DIHE	C11	C12	C13	N1	! dihe	178.9870
DIHE	H13	C12	C13	N1	! dihe	-0.4165
DIHE	C11	C12	C13	C14	! dihe	-0.5822
DIHE	H13	C12	C13	C14	! dihe	-179.9856
DIHE	N1	C13	C14	C2	! dihe	-0.0395
DIHE	C12	C13	C14	C2	! dihe	179.6379
DIHE	N1	C13	C14	C9	! dihe	-179.1001
DIHE	C12	C13	C14	C9	! dihe	0.5774
DIHE	C6	C16	N3	C17	! dihe	-2.9465
DIHE	O1	C16	N3	C17	! dihe	177.8537
DIHE	C6	C16	N3	C19	! dihe	178.1916
DIHE	O1	C16	N3	C19	! dihe	-1.0082
DIHE	C16	N3	C17	C18	! dihe	-94.0723
DIHE	C19	N3	C17	C18	! dihe	84.7949
DIHE	C16	N3	C17	H17	! dihe	144.6045
DIHE	C19	N3	C17	H17	! dihe	-36.5284
DIHE	C16	N3	C17	H18	! dihe	30.0345
DIHE	C19	N3	C17	H18	! dihe	-151.0983
DIHE	C16	N3	C19	C20	! dihe	-85.6776
DIHE	C17	N3	C19	C20	! dihe	95.3585
DIHE	C16	N3	C19	H22	! dihe	152.6736
DIHE	C17	N3	C19	H22	! dihe	-26.2902
DIHE	C16	N3	C19	H23	! dihe	36.6643
DIHE	C17	N3	C19	H23	! dihe	-142.2996
DIHE	N3	C17	C18	H19	! dihe	-177.5392
DIHE	H17	C17	C18	H19	! dihe	-57.7765
DIHE	H18	C17	C18	H19	! dihe	58.3389
DIHE	N3	C17	C18	H20	! dihe	62.4644
DIHE	H17	C17	C18	H20	! dihe	-177.7728
DIHE	H18	C17	C18	H20	! dihe	-61.6575
DIHE	N3	C17	C18	H21	! dihe	-57.7923
DIHE	H17	C17	C18	H21	! dihe	61.9704
DIHE	H18	C17	C18	H21	! dihe	178.0858
DIHE	N3	C19	C20	H24	! dihe	-178.0851
DIHE	H22	C19	C20	H24	! dihe	-58.3100
DIHE	H23	C19	C20	H24	! dihe	60.6723
DIHE	N3	C19	C20	H25	! dihe	62.5026
DIHE	H22	C19	C20	H25	! dihe	-177.7223
DIHE	H23	C19	C20	H25	! dihe	-58.7400
DIHE	N3	C19	C20	H26	! dihe	-58.5561
DIHE	H22	C19	C20	H26	! dihe	61.2189
DIHE	H23	C19	C20	H26	! dihe	-179.7987
IMPH	C13	C1	N1	H1		
IMPH	C2	H2	C1	N1		
IMPH	C3	C14	C2	C1		
IMPH	C6	C8	C7	H10		
IMPH	C7	C4	C8	C9		
IMPH	C10	C14	C9	C8		
IMPH	C9	C11	C10	H11		

```

IMPH C10    C12    C11    H12
IMPH C11    C13    C12    H13
IMPH C12    C14    C13    N1
IMPH C9     C13    C14    C2
IMPH C6     N3     C16    O1
IMPH C16    C17    N3     C19

```

Parameter file for LSD

```

* Force Field Parameter File.
*
```

BOND

```

lcc lna  438.80  1.371
lca lna  470.30  1.350
lnh lna  406.60  1.011
lcc lcd  504.00  1.371
lcc lh4  350.10  1.083
lc3 lcd  337.30  1.499
lca lcd  411.70  1.434
lc3 lc3  303.10  1.535
lc3 lhc  337.30  1.092
lc3 ln4  293.60  1.499
lc3 lce  331.30  1.505
lc3 lhx  338.70  1.091
lnh ln4  369.00  1.033
lc2 lc3  328.30  1.508
lc  lc3  328.30  1.508
lc2 lce  560.50  1.339
lc2 lha  344.30  1.087
lca lce  366.00  1.472
lca lca  478.40  1.387
lca lha  344.30  1.087
lc  lo   648.00  1.214
lc  ln   478.20  1.345
lc3 ln   330.60  1.460
lc3 lh1  335.90  1.093

```

ANGLE

```

lna lcc lcd  72.900  109.420
lna lcc lh4  50.200  119.660
lna lca lca  70.200  118.340
lcc lna lca  68.500  113.150
lcc lna lhn  47.200  124.660
lcc lcd lc3  64.800  119.450
lcc lcd lca  68.200  113.510
lcd lcc lh4  47.200  129.110
lcd lc3 lc3  64.700  108.100
lcd lc3 lhc  47.200  110.860
lcd lca lca  66.000  120.100
lc3 lcd lca  64.100  117.810
lc3 lc3 ln4  66.000  108.930
lc3 lc3 lce  63.700  110.960 ! same as lc2 lc3 lc3
lc3 lc3 lhx  46.000  111.740
lc3 lc3 lhc  46.400  110.050
lc3 ln4 lc3  62.800  110.640

```

lc3	ln4	lnh	46.200	110.110
lc3	lce	lc2	64.300	122.890
lc3	lce	lca	63.200	117.620
ln4	lc3	lce	65.845	111.515 ! Calculated with empirical approach
ln4	lc3	lhx	49.000	107.910
lc3	lc3	lc2	63.700	110.960
lc3	lc3	lc	63.800	110.530
lc3	lc2	lce	65.700	117.400
lc3	lc2	lha	45.700	117.300
lc3	lc	lo	68.000	123.110
lc3	lc	ln	67.900	115.150
lc2	lc3	lc	64.600	109.730
lc2	lc3	lhc	47.000	110.490
lc2	lce	lca	65.200	123.080
lce	lc3	lhx	47.000	110.980 ! same as lce lc3 lhc
lce	lc2	lha	49.600	121.190
lce	lca	lca	64.900	120.660
lca	lca	lca	67.200	119.970
lca	lca	lha	48.500	120.010
lca	lna	lnh	48.200	122.770
lc	lc3	lhc	47.200	109.680
lc	ln	lc3	63.900	121.350
lo	lc	ln	75.800	122.030
ln	lc3	lc3	65.900	112.130
ln	lc3	lh1	49.800	109.320
lc3	ln	lc3	64.000	112.620
lc3	lc3	lh1	46.400	110.070
lhc	lc3	lhc	39.400	108.350
lhx	lc3	lhx	39.000	110.740
lh1	lc3	lh1	39.200	109.550

DIHEDRAL

X	lcc	lna	X	1.700	2	180.0
X	lca	lna	X	0.300	2	180.0
X	lcc	lcd	X	4.000	2	180.0
X	lc3	lcd	X	0.000	3	0.0
lcc	lcd	lca	lca	2.550	2	180.0 ! same as X lc2 lca X
lc3	lcd	lca	lca	2.550	2	180.0 ! same as X lc2 lca X
X	lc3	lc3	X	0.156	3	0.0
X	lc3	ln4	X	0.156	3	0.0
lc3	lc3	lce	lc2	0.000	2	0.0 ! same as X lc2 lc3 X
ln4	lc3	lce	lc2	0.000	2	0.0 ! same as X lc2 lc3 X
lhx	lc3	lce	lc2	0.000	2	0.0 ! same as X lc2 lc3 X
lc3	lc3	lce	lca	0.000	2	0.0 ! same as X lc2 lc3 X
ln4	lc3	lce	lca	0.000	2	0.0 ! same as X lc2 lc3 X
lhx	lc3	lce	lca	0.000	2	0.0 ! same as X lc2 lc3 X
X	lc2	lc3	X	0.000	2	0.0
X	lc	lc3	X	0.000	2	180.0
lhc	lc3	lc	lo	0.800	1	0.0
lhc	lc3	lc	lo	0.080	3	180.0
lc3	lc3	lc	ln	0.100	4	0.0
lc3	lc3	lc	ln	0.070	2	0.0
X	lc2	lce	X	6.650	2	180.0
lc3	lce	lca	lca	2.550	2	180.0 ! same as X lc2 lca X
lc2	lce	lca	lca	2.550	2	180.0 ! same as X lc2 lca X
X	lca	lca	X	3.625	2	180.0

X	lc	ln	X	2.500	2	180.0
X	lc3	ln	X	0.000	2	0.0
lc3	lc3	ln	lc	0.500	4	180.0
lc3	lc3	ln	lc	0.150	3	180.0
lc3	lc3	ln	lc	0.530	1	0.0
IMPHI						
X	X	lna	lnh	1.100	0	180.0
lcd	lh4	lcc	lna	1.100	0	180.0 ! Using default value
lc3	lca	lcd	lcc	1.100	0	180.0 ! Using default value
lc3	lce	lc2	lha	1.100	0	180.0 ! Using default value
lc2	lc3	lce	lca	1.100	0	180.0 ! Using default value
lca	lca	lca	lce	1.100	0	180.0 ! Using default value
X	X	lca	lha	1.100	0	180.0
lca	lca	lca	lna	1.100	0	180.0 ! Using default value
lca	lca	lca	lcd	1.100	0	180.0 ! Using default value
X	X	lc	lo	10.500	0	180.0
X	lc3	ln	lc3	1.100	0	180.0
NONBONDED NBXMOD 5 GROUP SWITCH CDIEL -						
CUTNB	14.0	CTOFNB	12.0	CTONNB	10.0	EPS 1.0 E14FAC 0.83333333 WMIN 1.4
! Emin Rmin/2 Emin/2 Rmin (for 1-4's)						
! (klcal/mol) (A)						
lna	0.00	-0.1700	1.8240	0.00	-0.0850	1.8240
lcc	0.00	-0.0860	1.9080	0.00	-0.0430	1.9080
lcd	0.00	-0.0860	1.9080	0.00	-0.0430	1.9080
lc3	0.00	-0.1094	1.9080	0.00	-0.0547	1.9080
ln4	0.00	-0.1700	1.8240	0.00	-0.0850	1.8240
lc2	0.00	-0.0860	1.9080	0.00	-0.0430	1.9080
lce	0.00	-0.0860	1.9080	0.00	-0.0430	1.9080
lca	0.00	-0.0860	1.9080	0.00	-0.0430	1.9080
lc	0.00	-0.0860	1.9080	0.00	-0.0430	1.9080
lo	0.00	-0.2100	1.6612	0.00	-0.1050	1.6612
ln	0.00	-0.1700	1.8240	0.00	-0.0850	1.8240
lnh	0.00	-0.0157	0.6000	0.00	-0.0078	0.6000
lh4	0.00	-0.0150	1.4090	0.00	-0.0075	1.4090
lhc	0.00	-0.0157	1.4870	0.00	-0.0078	1.4870
lhx	0.00	-0.0157	1.1000	0.00	-0.0078	1.1000
lha	0.00	-0.0150	1.4590	0.00	-0.0075	1.4590
lh1	0.00	-0.0157	1.3870	0.00	-0.0078	1.3870

Topology file for KET

* Topology File.

*

99	1		
MASS	301	lca	12.010000
MASS	302	ln	14.010000
MASS	303	lc	12.010000
MASS	304	lo	16.000000
MASS	305	lc3	12.010000
MASS	306	ln4	14.010000
MASS	307	lf	19.000000
MASS	308	lha	1.008000
MASS	309	lnh	1.008000
MASS	310	lh1	1.008000

MASS 311 lhx 1.008000
MASS 312 lhc 1.008000

RESI Ket 1.000
GROUP
ATOM C1 lca -0.296815
ATOM C2 lca -0.009884
ATOM H1 lha 0.153986
ATOM C3 lca -0.234728
ATOM H2 lha 0.171015
ATOM C4 lca -0.003149
ATOM H3 lha 0.158239
ATOM C5 lca -0.350382
ATOM H4 lha 0.195082
ATOM C6 lca 0.425274
ATOM N1 ln -0.699757
ATOM H5 lhn 0.417204
ATOM C7 lc 0.749952
ATOM O2 lo -0.597216
ATOM N2 ln -0.158072
ATOM C8 lc 0.643682
ATOM O1 lo -0.549078
GROUP
ATOM C9 lc3 -0.155669
ATOM H6 lh1 0.134469
ATOM H7 lh1 0.134469
GROUP
ATOM C10 lc3 -0.419263
ATOM H8 lhx 0.210798
ATOM H9 lhx 0.210798
GROUP
ATOM N3 ln4 0.008466
ATOM H23 lhn 0.351961
ATOM C11 lc3 -0.170616
ATOM H10 lhx 0.148541
ATOM H11 lhx 0.148541
ATOM C12 lc3 0.116796
ATOM H12 lhc 0.019894
ATOM H13 lhc 0.019894
ATOM C13 lc3 -0.243043
ATOM H14 lhc 0.035438
ATOM C14 lc3 0.116796
ATOM H15 lhc 0.019894
ATOM H16 lhc 0.019894
ATOM C15 lc3 -0.170616
ATOM H17 lhx 0.148541
ATOM H18 lhx 0.148541
GROUP
ATOM C16 lc 0.633248
ATOM O3 lo -0.507103
GROUP
ATOM C17 lca -0.218661
ATOM C18 lca -0.031968
ATOM H19 lha 0.164206
ATOM C19 lca -0.366092
ATOM H20 lha 0.203795

ATOM	C20	lca	0.515454
ATOM	F1	lf	-0.212696
ATOM	C21	lca	-0.366092
ATOM	H21	lha	0.203795
ATOM	C22	lca	-0.031968
ATOM	H22	lha	0.164206
BOND	C1	C2	! dist 1.3957
BOND	C1	C6	! dist 1.3885
BOND	C1	C8	! dist 1.4652
BOND	C2	C3	! dist 1.3748
BOND	C2	H1	! dist 1.0729
BOND	C3	C4	! dist 1.3944
BOND	C3	H2	! dist 1.0736
BOND	C4	C5	! dist 1.3792
BOND	C4	H3	! dist 1.0753
BOND	C5	C6	! dist 1.3896
BOND	C5	H4	! dist 1.0749
BOND	C6	N1	! dist 1.3899
BOND	N1	C7	! dist 1.3521
BOND	N1	H5	! dist 0.9974
BOND	C7	N2	! dist 1.3872
BOND	C7	O2	! dist 1.1997
BOND	N2	C8	! dist 1.3980
BOND	N2	C9	! dist 1.4503
BOND	C8	O1	! dist 1.1975
BOND	C9	C10	! dist 1.5290
BOND	C9	H6	! dist 1.0802
BOND	C9	H7	! dist 1.0762
BOND	C10	N3	! dist 1.5008
BOND	C10	H8	! dist 1.0806
BOND	C10	H9	! dist 1.0781
BOND	N3	C11	! dist 1.5058
BOND	N3	C15	! dist 1.5035
BOND	N3	H23	! dist 1.0104
BOND	C11	C12	! dist 1.5223
BOND	C11	H10	! dist 1.0821
BOND	C11	H11	! dist 1.0809
BOND	C12	C13	! dist 1.5315
BOND	C12	H12	! dist 1.0839
BOND	C12	H13	! dist 1.0839
BOND	C13	C14	! dist 1.5388
BOND	C13	C16	! dist 1.5339
BOND	C13	H14	! dist 1.0841
BOND	C14	C15	! dist 1.5240
BOND	C14	H15	! dist 1.0831
BOND	C14	H16	! dist 1.0862
BOND	C15	H17	! dist 1.0822
BOND	C15	H18	! dist 1.0796
BOND	C16	O3	! dist 1.1965
BOND	C16	C17	! dist 1.4878
BOND	C17	C18	! dist 1.3979
BOND	C17	C22	! dist 1.3932
BOND	C18	C19	! dist 1.3772
BOND	C18	H19	! dist 1.0730
BOND	C19	C20	! dist 1.3821

BOND	C19	H20	! dist	1.0736
BOND	C20	C21	! dist	1.3797
BOND	C20	F1	! dist	1.3178
BOND	C21	C22	! dist	1.3827
BOND	C21	H21	! dist	1.0739
BOND	C22	H22	! dist	1.0732
ANGL	C1	C2	C3	! angle 120.0613
ANGL	C1	C2	H1	! angle 118.5739
ANGL	C1	C6	C5	! angle 120.2533
ANGL	C1	C6	N1	! angle 118.8086
ANGL	C1	C8	N2	! angle 115.3585
ANGL	C1	C8	O1	! angle 125.0444
ANGL	C2	C1	C6	! angle 119.9852
ANGL	C2	C1	C8	! angle 120.3846
ANGL	C2	C3	C4	! angle 119.3514
ANGL	C2	C3	H2	! angle 120.5079
ANGL	C3	C2	H1	! angle 121.3643
ANGL	C3	C4	C5	! angle 121.3653
ANGL	C3	C4	H3	! angle 119.6287
ANGL	C4	C3	H2	! angle 120.1407
ANGL	C4	C5	C6	! angle 118.9831
ANGL	C4	C5	H4	! angle 120.7117
ANGL	C5	C4	H3	! angle 119.0059
ANGL	C5	C6	N1	! angle 120.9344
ANGL	C6	C1	C8	! angle 119.6303
ANGL	C6	C5	H4	! angle 120.3052
ANGL	C6	N1	C7	! angle 124.9950
ANGL	C6	N1	H5	! angle 120.0449
ANGL	N1	C7	N2	! angle 115.6285
ANGL	N1	C7	O2	! angle 123.3309
ANGL	C7	N1	H5	! angle 114.9443
ANGL	C7	N2	C8	! angle 125.2856
ANGL	C7	N2	C9	! angle 116.6218
ANGL	N2	C7	O2	! angle 121.0385
ANGL	N2	C8	O1	! angle 119.5971
ANGL	N2	C9	C10	! angle 109.7366
ANGL	N2	C9	H6	! angle 107.9502
ANGL	N2	C9	H7	! angle 107.2390
ANGL	C8	N2	C9	! angle 118.0803
ANGL	C9	C10	N3	! angle 112.5573
ANGL	C9	C10	H8	! angle 111.2117
ANGL	C9	C10	H9	! angle 109.3092
ANGL	C10	C9	H6	! angle 110.4212
ANGL	C10	C9	H7	! angle 111.6494
ANGL	C10	N3	C11	! angle 111.1693
ANGL	C10	N3	C15	! angle 113.3797
ANGL	C10	N3	H23	! angle 106.9220
ANGL	N3	C10	H8	! angle 107.4877
ANGL	N3	C10	H9	! angle 106.4381
ANGL	N3	C11	C12	! angle 111.0396
ANGL	N3	C11	H10	! angle 106.2272
ANGL	N3	C11	H11	! angle 107.0161
ANGL	N3	C15	C14	! angle 111.1625
ANGL	N3	C15	H17	! angle 106.2238
ANGL	N3	C15	H18	! angle 107.9048

ANGL	C11	N3	C15	! angle	110.7736
ANGL	C11	N3	H23	! angle	106.6925
ANGL	C11	C12	C13	! angle	111.8172
ANGL	C11	C12	H12	! angle	107.7454
ANGL	C11	C12	H13	! angle	110.2168
ANGL	C12	C11	H10	! angle	112.2942
ANGL	C12	C11	H11	! angle	111.3429
ANGL	C12	C13	C14	! angle	109.3965
ANGL	C12	C13	C16	! angle	110.2166
ANGL	C12	C13	H14	! angle	108.6815
ANGL	C13	C12	H12	! angle	110.6653
ANGL	C13	C12	H13	! angle	109.7860
ANGL	C13	C14	C15	! angle	112.1187
ANGL	C13	C14	H15	! angle	111.2552
ANGL	C13	C14	H16	! angle	109.3139
ANGL	C13	C16	O3	! angle	117.9338
ANGL	C13	C16	C17	! angle	120.6142
ANGL	C14	C13	C16	! angle	108.9928
ANGL	C14	C13	H14	! angle	108.9968
ANGL	C14	C15	H17	! angle	111.9980
ANGL	C14	C15	H18	! angle	110.8565
ANGL	C15	N3	H23	! angle	107.5344
ANGL	C15	C14	H15	! angle	107.6065
ANGL	C15	C14	H16	! angle	109.6451
ANGL	C16	C13	H14	! angle	110.5340
ANGL	C16	C17	C18	! angle	117.4262
ANGL	C16	C17	C22	! angle	123.8086
ANGL	O3	C16	C17	! angle	121.4122
ANGL	C17	C18	C19	! angle	120.9951
ANGL	C17	C18	H19	! angle	118.8562
ANGL	C17	C22	C21	! angle	120.9420
ANGL	C17	C22	H22	! angle	121.2964
ANGL	C18	C17	C22	! angle	118.7641
ANGL	C18	C19	C20	! angle	118.5252
ANGL	C18	C19	H20	! angle	121.8209
ANGL	C19	C18	H19	! angle	120.1486
ANGL	C19	C20	C21	! angle	122.2866
ANGL	C19	C20	F1	! angle	118.9468
ANGL	C20	C19	H20	! angle	119.6539
ANGL	C20	C21	C22	! angle	118.4867
ANGL	C20	C21	H21	! angle	119.6968
ANGL	C21	C20	F1	! angle	118.7665
ANGL	C21	C22	H22	! angle	117.7612
ANGL	C22	C21	H21	! angle	121.8160
ANGL	H6	C9	H7	! angle	109.7241
ANGL	H8	C10	H9	! angle	109.6969
ANGL	H10	C11	H11	! angle	108.6482
ANGL	H12	C12	H13	! angle	106.4539
ANGL	H15	C14	H16	! angle	106.7441
ANGL	H17	C15	H18	! angle	108.4901
DIHE	C6	C1	C2	C3	! dihe -0.2091
DIHE	C8	C1	C2	C3	! dihe 179.7343
DIHE	C6	C1	C2	H1	! dihe -179.9608
DIHE	C8	C1	C2	H1	! dihe -0.0173
DIHE	C2	C1	C6	C5	! dihe 0.0295

DIHE	C8	C1	C6	C5	! dihe	-179.9144
DIHE	C2	C1	C6	N1	! dihe	-179.2775
DIHE	C8	C1	C6	N1	! dihe	0.7786
DIHE	C2	C1	C8	N2	! dihe	-177.0884
DIHE	C6	C1	C8	N2	! dihe	2.8553
DIHE	C2	C1	C8	O1	! dihe	2.9628
DIHE	C6	C1	C8	O1	! dihe	-177.0936
DIHE	C1	C2	C3	C4	! dihe	0.2212
DIHE	H1	C2	C3	C4	! dihe	179.9657
DIHE	C1	C2	C3	H2	! dihe	-179.7969
DIHE	H1	C2	C3	H2	! dihe	-0.0523
DIHE	C2	C3	C4	C5	! dihe	-0.0564
DIHE	H2	C3	C4	C5	! dihe	179.9615
DIHE	C2	C3	C4	H3	! dihe	-179.9721
DIHE	H2	C3	C4	H3	! dihe	0.0458
DIHE	C3	C4	C5	C6	! dihe	-0.1211
DIHE	H3	C4	C5	C6	! dihe	179.7952
DIHE	C3	C4	C5	H4	! dihe	179.9757
DIHE	H3	C4	C5	H4	! dihe	-0.1081
DIHE	C4	C5	C6	C1	! dihe	0.1333
DIHE	H4	C5	C6	C1	! dihe	-179.9631
DIHE	C4	C5	C6	N1	! dihe	179.4253
DIHE	H4	C5	C6	N1	! dihe	-0.6710
DIHE	C1	C6	N1	C7	! dihe	-1.4536
DIHE	C5	C6	N1	C7	! dihe	179.2443
DIHE	C1	C6	N1	H5	! dihe	177.0277
DIHE	C5	C6	N1	H5	! dihe	-2.2743
DIHE	C6	N1	C7	N2	! dihe	-1.6968
DIHE	H5	N1	C7	N2	! dihe	179.7531
DIHE	C6	N1	C7	O2	! dihe	177.7721
DIHE	H5	N1	C7	O2	! dihe	-0.7781
DIHE	N1	C7	N2	C8	! dihe	5.9562
DIHE	O2	C7	N2	C8	! dihe	-173.5259
DIHE	N1	C7	N2	C9	! dihe	-175.3466
DIHE	O2	C7	N2	C9	! dihe	5.1713
DIHE	C7	N2	C8	C1	! dihe	-6.4955
DIHE	C9	N2	C8	C1	! dihe	174.8246
DIHE	C7	N2	C8	O1	! dihe	173.4564
DIHE	C9	N2	C8	O1	! dihe	-5.2235
DIHE	C7	N2	C9	C10	! dihe	-84.8688
DIHE	C8	N2	C9	C10	! dihe	93.9258
DIHE	C7	N2	C9	H6	! dihe	35.5216
DIHE	C8	N2	C9	H6	! dihe	-145.6837
DIHE	C7	N2	C9	H7	! dihe	153.6838
DIHE	C8	N2	C9	H7	! dihe	-27.5215
DIHE	N2	C9	C10	N3	! dihe	167.6199
DIHE	H6	C9	C10	N3	! dihe	48.7409
DIHE	H7	C9	C10	N3	! dihe	-73.6191
DIHE	N2	C9	C10	H8	! dihe	-71.6993
DIHE	H6	C9	C10	H8	! dihe	169.4218
DIHE	H7	C9	C10	H8	! dihe	47.0618
DIHE	N2	C9	C10	H9	! dihe	49.5708
DIHE	H6	C9	C10	H9	! dihe	-69.3081
DIHE	H7	C9	C10	H9	! dihe	168.3318
DIHE	C9	C10	N3	C11	! dihe	-168.4774
DIHE	H8	C10	N3	C11	! dihe	68.7269

DIHE H9	C10	N3	C11	! dihe	-48.7501
DIHE C9	C10	N3	C15	! dihe	65.9466
DIHE H8	C10	N3	C15	! dihe	-56.8491
DIHE H9	C10	N3	C15	! dihe	-174.3260
DIHE C9	C10	N3	H23	! dihe	-52.3875
DIHE H8	C10	N3	H23	! dihe	-175.1832
DIHE H9	C10	N3	H23	! dihe	67.3399
DIHE C10	N3	C11	C12	! dihe	175.4096
DIHE C15	N3	C11	C12	! dihe	-57.5751
DIHE H23	N3	C11	C12	! dihe	59.1785
DIHE C10	N3	C11	H10	! dihe	-62.2278
DIHE C15	N3	C11	H10	! dihe	64.7875
DIHE H23	N3	C11	H10	! dihe	-178.4589
DIHE C10	N3	C11	H11	! dihe	53.7065
DIHE C15	N3	C11	H11	! dihe	-179.2782
DIHE H23	N3	C11	H11	! dihe	-62.5246
DIHE C10	N3	C15	C14	! dihe	-177.3110
DIHE C11	N3	C15	C14	! dihe	56.9018
DIHE H23	N3	C15	C14	! dihe	-59.3317
DIHE C10	N3	C15	H17	! dihe	60.6184
DIHE C11	N3	C15	H17	! dihe	-65.1688
DIHE H23	N3	C15	H17	! dihe	178.5977
DIHE C10	N3	C15	H18	! dihe	-55.5566
DIHE C11	N3	C15	H18	! dihe	178.6562
DIHE H23	N3	C15	H18	! dihe	62.4227
DIHE N3	C11	C12	C13	! dihe	57.0625
DIHE H10	C11	C12	C13	! dihe	-61.7085
DIHE H11	C11	C12	C13	! dihe	176.2018
DIHE N3	C11	C12	H12	! dihe	178.8813
DIHE H10	C11	C12	H12	! dihe	60.1103
DIHE H11	C11	C12	H12	! dihe	-61.9794
DIHE N3	C11	C12	H13	! dihe	-65.3482
DIHE H10	C11	C12	H13	! dihe	175.8807
DIHE H11	C11	C12	H13	! dihe	53.7910
DIHE C11	C12	C13	C14	! dihe	-54.2999
DIHE H12	C12	C13	C14	! dihe	-174.4238
DIHE H13	C12	C13	C14	! dihe	68.3566
DIHE C11	C12	C13	C16	! dihe	-174.1243
DIHE H12	C12	C13	C16	! dihe	65.7519
DIHE H13	C12	C13	C16	! dihe	-51.4677
DIHE C11	C12	C13	H14	! dihe	64.6041
DIHE H12	C12	C13	H14	! dihe	-55.5198
DIHE H13	C12	C13	H14	! dihe	-172.7393
DIHE C12	C13	C14	C15	! dihe	53.7369
DIHE C16	C13	C14	C15	! dihe	174.3102
DIHE H14	C13	C14	C15	! dihe	-64.9715
DIHE C12	C13	C14	H15	! dihe	174.2967
DIHE C16	C13	C14	H15	! dihe	-65.1300
DIHE H14	C13	C14	H15	! dihe	55.5883
DIHE C12	C13	C14	H16	! dihe	-68.0651
DIHE C16	C13	C14	H16	! dihe	52.5083
DIHE H14	C13	C14	H16	! dihe	173.2265
DIHE C12	C13	C16	O3	! dihe	31.2247
DIHE C14	C13	C16	O3	! dihe	-88.8436
DIHE H14	C13	C16	O3	! dihe	151.3856
DIHE C12	C13	C16	C17	! dihe	-151.0349

DIHE	C14	C13	C16	C17	! dihe	88.8968
DIHE	H14	C13	C16	C17	! dihe	-30.8741
DIHE	C13	C14	C15	N3	! dihe	-55.7707
DIHE	H15	C14	C15	N3	! dihe	-178.4226
DIHE	H16	C14	C15	N3	! dihe	65.8417
DIHE	C13	C14	C15	H17	! dihe	62.8828
DIHE	H15	C14	C15	H17	! dihe	-59.7692
DIHE	H16	C14	C15	H17	! dihe	-175.5049
DIHE	C13	C14	C15	H18	! dihe	-175.7889
DIHE	H15	C14	C15	H18	! dihe	61.5591
DIHE	H16	C14	C15	H18	! dihe	-54.1766
DIHE	C13	C16	C17	C18	! dihe	-177.5457
DIHE	O3	C16	C17	C18	! dihe	0.1151
DIHE	C13	C16	C17	C22	! dihe	2.0658
DIHE	O3	C16	C17	C22	! dihe	179.7265
DIHE	C16	C17	C18	C19	! dihe	179.7657
DIHE	C22	C17	C18	C19	! dihe	0.1340
DIHE	C16	C17	C18	H19	! dihe	-0.3415
DIHE	C22	C17	C18	H19	! dihe	-179.9733
DIHE	C16	C17	C22	C21	! dihe	-179.6057
DIHE	C18	C17	C22	C21	! dihe	0.0009
DIHE	C16	C17	C22	H22	! dihe	0.6042
DIHE	C18	C17	C22	H22	! dihe	-179.7891
DIHE	C17	C18	C19	C20	! dihe	-0.1744
DIHE	H19	C18	C19	C20	! dihe	179.9342
DIHE	C17	C18	C19	H20	! dihe	179.8817
DIHE	H19	C18	C19	H20	! dihe	-0.0098
DIHE	C18	C19	C20	C21	! dihe	0.0833
DIHE	H20	C19	C20	C21	! dihe	-179.9715
DIHE	C18	C19	C20	F1	! dihe	-179.9848
DIHE	H20	C19	C20	F1	! dihe	-0.0396
DIHE	C19	C20	C21	C22	! dihe	0.0473
DIHE	F1	C20	C21	C22	! dihe	-179.8847
DIHE	C19	C20	C21	H21	! dihe	179.8181
DIHE	F1	C20	C21	H21	! dihe	-0.1139
DIHE	C20	C21	C22	C17	! dihe	-0.0891
DIHE	H21	C21	C22	C17	! dihe	-179.8548
DIHE	C20	C21	C22	H22	! dihe	179.7081
DIHE	H21	C21	C22	H22	! dihe	-0.0575
IMPH	C8	C6	C1	C2		
IMPH	C1	C3	C2	H1		
IMPH	C2	C4	C3	H2		
IMPH	C3	C5	C4	H3		
IMPH	C4	C6	C5	H4		
IMPH	C1	C5	C6	N1		
IMPH	C7	C6	N1	H5		
IMPH	N1	N2	C7	O2		
IMPH	C7	C8	N2	C9		
IMPH	C1	N2	C8	O1		
IMPH	C13	C17	C16	O3		
IMPH	C16	C18	C17	C22		
IMPH	C17	C19	C18	H19		
IMPH	C18	C20	C19	H20		
IMPH	C19	C21	C20	F1		
IMPH	C20	C22	C21	H21		

IMPH C17 C21 C22 H22

Parameter file for KET

* Force Field Parameter File.
*

BOND

lca lca	478.40	1.387
lc lca	349.70	1.487
lca lha	344.30	1.087
lca ln	372.30	1.422
lc ln	478.20	1.345
lnh ln	410.20	1.009
lc lo	648.00	1.214
lc3 ln	330.60	1.460
lc3 lc3	303.10	1.535
lc3 lh1	335.90	1.093
lc3 ln4	293.60	1.499
lc3 lhx	338.70	1.091
lnh ln4	369.00	1.033
lc3 lhc	337.30	1.092
lc lc3	328.30	1.508
lca lf	363.80	1.344

ANGLE

lca lca lca	67.200	119.970
lca lca lha	48.500	120.010
lca lca ln	68.000	119.890
lca lc ln	69.400	112.030
lca lc lo	68.700	123.440
lca lca lc	64.600	120.140
lca ln lc	64.300	123.710
lca ln lhn	47.600	114.590
ln lc ln	75.400	111.700
ln lc lo	75.800	122.030
lc ln lhn	49.200	118.460
lc ln lc	67.400	119.630
lc ln lc3	63.900	121.350
ln lc3 lc3	65.900	112.130
ln lc3 lh1	49.800	109.320
lc3 lc3 ln4	66.000	108.930
lc3 lc3 lhx	46.000	111.740
lc3 lc3 lh1	46.400	110.070
lc3 ln4 lc3	62.800	110.640
lc3 ln4 lhn	46.200	110.110
ln4 lc3 lhx	49.000	107.910
lc3 lc3 lc3	63.200	110.630
lc3 lc3 lhc	46.400	110.050
lc3 lc3 lc	63.800	110.530
lc3 lc lo	68.000	123.110
lc3 lc lca	62.300	119.530
lc lc3 lhc	47.200	109.680
lca lca lf	67.600	118.740
lh1 lc3 lh1	39.200	109.550
lhx lc3 lhx	39.000	110.740

lhc lc3 lhc 39.400 108.350

DIHEDRAL

X	lca	lca	X	3.625	2	180.0
X	lc	lca	X	3.625	2	180.0
X	lca	ln	X	0.450	2	180.0
X	lc	ln	X	2.500	2	180.0
lhn	ln	lc	lo	2.500	2	180.0
lhn	ln	lc	lo	2.000	1	0.0
X	lc3	ln	X	0.000	2	0.0
lc3	lc3	ln	lc	0.500	4	180.0
lc3	lc3	ln	lc	0.150	3	180.0
lc3	lc3	ln	lc	0.530	1	0.0
X	lc3	lc3	X	0.156	3	0.0
X	lc3	ln4	X	0.156	3	0.0
lc3	lc3	lc3	lc3	0.180	3	0.0
lc3	lc3	lc3	lc3	0.250	2	180.0
lc3	lc3	lc3	lc3	0.200	1	180.0
lhc	lc3	lc3	lc3	0.160	3	0.0
lhc	lc3	lc3	lhc	0.150	3	0.0
X	lc	lc3	X	0.000	2	180.0
lhc	lc3	lc	lo	0.800	1	0.0
lhc	lc3	lc	lo	0.080	3	180.0

IMPHI

lc	lca	lca	lca	1.100	0	180.0	! Using default value
X	X	lca	lha	1.100	0	180.0	
lca	lca	lca	ln	1.100	0	180.0	! Using default value
X	X	ln	lhn	1.100	0	180.0	
X	X	lc	lo	10.500	0	180.0	
lc	lc	ln	lc3	1.100	0	180.0	! Using default value
lca	lca	lca	lf	1.100	0	180.0	

NONBONDED NBXMOD 5 GROUP SWITCH CDIEL -

CUTNB	14.0	CTOFNB	12.0	CTONNB	10.0	EPS	1.0	E14FAC	0.83333333	WMIN	1.4
				Emin		Rmin/2		Emin/2		Rmin (lfor 1-4's)	
				(klcal/mol)		(Å)					
!											
lca	0.00	-0.0860	1.9080	0.00	-0.0430	1.9080					
ln	0.00	-0.1700	1.8240	0.00	-0.0850	1.8240					
lc	0.00	-0.0860	1.9080	0.00	-0.0430	1.9080					
lo	0.00	-0.2100	1.6612	0.00	-0.1050	1.6612					
lc3	0.00	-0.1094	1.9080	0.00	-0.0547	1.9080					
ln4	0.00	-0.1700	1.8240	0.00	-0.0850	1.8240					
lf	0.00	-0.0610	1.7500	0.00	-0.0305	1.7500					
lha	0.00	-0.0150	1.4590	0.00	-0.0075	1.4590					
ln	0.00	-0.0157	0.6000	0.00	-0.0078	0.6000					
lh1	0.00	-0.0157	1.3870	0.00	-0.0078	1.3870					
lhx	0.00	-0.0157	1.1000	0.00	-0.0078	1.1000					
lhc	0.00	-0.0157	1.4870	0.00	-0.0078	1.4870					

Supplemental References

1. Shan J, Weinstein H, Mehler EL (2010) Probing the Structural Determinants for the Function of Intracellular Loop 2 in Structurally Cognate G-Protein-Coupled Receptors. *Biochemistry* 49: 10691-10701.
2. Kortagere S, Roy A, Mehler EL (2006) Ab initio computational modeling of long loops in G-protein coupled receptors. *J Comput Aided Mol Des* 20: 427-436.
3. Mehler EL, Hassan SA, Kortagere S, Weinstein H (2006) *Ab initio* computational modeling of loops in G-protein-coupled receptors: lessons from the crystal structure of rhodopsin. *Proteins* 64: 673-690.
4. Mehler EL, Periole X, Hassan SA, Weinstein H (2002) Key issues in the computational simulation of GPCR function: representation of loop domains. *J Comput Aided Mol Des* 16: 841-853.
5. Okada T, Sugihara M, Bondar AN, Elstner M, Entel P, et al. (2004) The retinal conformation and its environment in rhodopsin in light of a new 2.2 Å crystal structure. *J Mol Biol* 342: 571-583.
6. Cherezov V, Rosenbaum DM, Hanson MA, Rasmussen SG, Thian FS, et al. (2007) High-resolution crystal structure of an engineered human β_2 -adrenergic G protein-coupled receptor. *Science* 318: 1258-1265.
7. Ballesteros JA, Weinstein H (1995) Integrated Methods for Modeling G-Protein Coupled Receptors. *Methods Neurosci* 25: 366-428.
8. Strader CD, Sigal IS, Dixon RA (1989) Structural basis of beta-adrenergic receptor function. *FASEB J* 3: 1825-1832.
9. Lan H, Liu Y, Bell MI, Gurevich VV, Neve KA (2009) A dopamine D2 receptor mutant capable of G protein-mediated signaling but deficient in arrestin binding. *Mol Pharmacol* 75: 113-123.
10. Bouvier M, Collins S, O'Dowd BF, Campbell PT, de Blasi A, et al. (1989) Two distinct pathways for cAMP-mediated down-regulation of the beta 2-adrenergic receptor. Phosphorylation of the receptor and regulation of its mRNA level. *J Biol Chem* 264: 16786-16792.
11. Bouvier M, Guilbault N, Bonin H (1991) Phorbol-ester-induced phosphorylation of the beta 2-adrenergic receptor decreases its coupling to Gs. *FEBS Lett* 279: 243-248.
12. Shapiro RA, Nathanson NM (1989) Deletion analysis of the mouse m1 muscarinic acetylcholine receptor: effects on phosphoinositide metabolism and down-regulation. *Biochemistry* 28: 8946-8950.
13. Keefer JR, Kennedy ME, Limbird LE (1994) Unique structural features important for stabilization versus polarization of the alpha 2A-adrenergic receptor on the basolateral membrane of Madin-Darby canine kidney cells. *J Biol Chem* 269: 16425-16432.
14. Schoneberg T, Liu J, Wess J (1995) Plasma membrane localization and functional rescue of truncated forms of a G protein-coupled receptor. *J Biol Chem* 270: 18000-18006.
15. Kobilka BK, Kobilka TS, Daniel K, Regan JW, Caron MG, et al. (1988) Chimeric alpha 2-,beta 2-adrenergic receptors: delineation of domains involved in effector coupling and ligand binding specificity. *Science* 240: 1310-1316.
16. Saunders C, Limbird LE (2000) Microtubule-dependent regulation of alpha(2B) adrenergic receptors in polarized MDCKII cells requires the third intracellular loop but not G protein coupling. *Mol Pharmacol* 57: 44-52.
17. Jaakola VP, Vainio M, Sen S, Rehn M, Heimo H, et al. (2005) Intracellularly truncated human alpha2B-adrenoceptors: stable and functional GPCRs for structural studies. *J Recept Signal Transduct Res* 25: 99-124.
18. Warne T, Serrano-Vega MJ, Baker JG, Moukhametzianov R, Edwards PC, et al. (2008) Structure of a β_1 -adrenergic G-protein-coupled receptor. *Nature* 454: 486-491.

19. Grossfield A, Feller SE, Pitman MC (2006) A role for direct interactions in the modulation of rhodopsin by omega-3 polyunsaturated lipids. *Proc Natl Acad Sci U S A* 103: 4888-4893.
20. Khelashvili G, Grossfield A, Feller SE, Pitman MC, Weinstein H (2009) Structural and dynamic effects of cholesterol at preferred sites of interaction with rhodopsin identified from microsecond length molecular dynamics simulations. *Proteins* 76: 403-417.